1

2

Anoxygenic Photosynthesis and Dark Carbon Metabolism under micro-oxic conditions in the Purple Sulfur Bacterium "*Thiodictyon syntrophicum*" nov. strain Cad16^T

6

7

8 Samuel M Luedin [1] [2] [3]*, Nicola Storelli [2], Francesco Danza [1] [2], Samuele Roman [2] [4],

9 Matthias Wittwer [3], Joël F Pothier [5] and Mauro Tonolla [1] [2] [4]‡

10

11

12 [1] Microbiology Unit, Department of Botany and Plant Biology, University of Geneva,
13 Geneva, Switzerland

14 [2] Laboratory of Applied Microbiology, Department of Environment, Constructions and
15 Design, University of Applied Sciences of Southern Switzerland (SUPSI), Bellinzona,
16 Switzerland

17 [3] Biology Division, Spiez Laboratory, Federal Office for Civil Protection, Spiez, Switzerland

18 [4] Alpine Biology Center Foundation, via Mirasole 22a, Bellinzona, Switzerland

19 [5] Environmental Genomics and System Biology Research Group, Institute of Natural
20 Resource Sciences, Zurich University of Applied Sciences (ZHAW), Wädenswil, Switzerland

21

22 Corresponding Authors

23 *Samuel Luedin
24 samuel.ludin@etu.unige.ch

25 ‡Prof. Mauro Tonolla
26 mauro.tonolla@supsi.ch

27

1. ABSTRACT

The microbial ecosystem of the meromictic Lake Cadagno (Ticino, Swiss Alps) has been studied intensively to understand metabolic functions driven by the highly abundant anoxygenic phototrophic sulfur bacteria of the families Chromatiaceae and Chlorobiaceae. It was found that the sequenced isolate "*Thiodictyon syntrophicum*" nov. sp. str. Cad16[T], belonging to the Chromatiaceae, may fix 26% of all bulk inorganic carbon in the chemocline at day and night. With this study, we elucidated the mode of dark carbon fixation of str. Cad16[T] with a combination of long-term monitoring of key physicochemical parameters with CTD, ^{14}C-incorporation experiments and quantitative proteomics of *in situ* dialysis bag incubations of pure cultures. Regular vertical CTD profiling during the study period in summer 2017 revealed that the chemocline sank from 12 to 14 m which was accompanied by a bloom of cyanobacteria and the subsequent oxygenation of the deeper water column. Sampling was performed both day and night in September. While CO_2 assimilation rates were higher during the light period, the relative change in the proteome (663 quantified proteins) was only 1% of all CDS encoded in str. Cad16[T]. Oxidative respiration was thereby upregulated at light, whereas stress-related mechanisms prevailed during the night. These results indicate that the low light availability due to high cell concentrations and the oxygenation of the chemocline induced a mixotrophic growth in str. Cad16[T].

The complete proteome data have been deposited to the ProteomeXchange with identifier PXD010641.

2. INTRODUCTION

Inorganic carbon, nitrogen and sulfur is cycled in diverse microbial metabolism networks in paired redox reactions and organic compounds are thereby produced in the scale of 10^9 t year^{-1} worldwide [1]. Light has been used as a source of energy in phototrophic anoxygenic bacteria since at least 3.85 Ga (billion years before the present) [2]. During carbon fixation, the transfer of electrons along a gradient of carrier molecules with sequentially lower potential allows the generation of energy bound to phosphate (ATP) and reductants [e.g., NAD(P)H and reduced ferredoxin]. The electrons required to replenish the oxidized electron acceptor pool can be derived from the oxidation of reduced sulfur species such as sulfide, sulfite and thiosulfate, or H_2 and Fe (II) [3].

The anoxygenic photosynthetic purple sulfur bacteria (PSB) of the family Chromatiaceae are found widespread in aquatic, sulfidic oxygen minimum-zones where light is still available [4]. As an adaption to low light availability around 0.1–20 μmol m^2 s^{-1} and only limited wavelength (450–600 nm, and infrared above 750 nm), PSB contain pigments of the carotenoid and bacteriochlorophyll *a* and *b* (BChl) classes [5], as well as multiple copies of antenna peptides (LHC), to subtly modulate charge separation within the membrane bound type II reaction center (RC) [6, 7]. Carbon is typically fixed through the Calvin-Benson-Bassham (CBB) cycle [8]. In order to store both, reduction-equivalents and oxidized carbon, PSB intracellularly concentrate elemental sulfur-chains (S-S_n^0) in protein covered globules (SGBs) [9] and glycogen and polyhydroxybutyrate (PHB) [10], respectively. These assimilates may subsequently allow for chemotrophic growth in the dark [11, 12].

The possibility of chemolithoautotrophic growth of PSB under microaerophilic conditions in the dark has been proposed by van Niel [13] and has been described first for *Thiocapsa roseopersicina* BBS [14]. The PSB *T. roseopersicina* inhabiting shallow tidal flats is especially adapted to the daily changes of oxygen concentrations and competes with chemotrophic non purple sulfur bacteria (*Thiobacillus* spp.) and *Beggiatoaceae* spp. [15]. Chemoheterotrophic, chemoautotrophic and mixotrophic growth has since been shown for different PSB spp. [16–21]. Several strains of *Allochromatium vinosum* and *T. roseopersicina* have shown mixotrophic growth under a 5% oxygen atmosphere and acetate, and different reduced sulfur compounds [18].

92   The ecological significance and the impact on biogeochemistry of PSB were extensively
93   studied in permanently stratified lakes [22–27]. In Lake Cadagno (Piora valley, Swiss Alps),
94   underwater springs in gypsum rich dolomite provide a steady inflow of solute-rich water. In
95   combination with solute-poor surface water, a stable and steep gradient in redox potential,
96   salinity, sulfide and oxygen concentrations at around 12 m depth is formed [28]. Within this
97   chemocline, a dense population of phototrophic sulfur oxidizing bacteria (PSOB) of the
98   family Chromatiaceae and Chlorobiaceae (GSB; green sulfur bacteria) thrive to dense
99   populations with up to 10^7 cells ml^{-1} between June and October [29]. *In situ* chemocline
100 incubation experiments with ^{14}C-uptake in Lake Cadagno [30, 31] and other lakes [32], as
101 well as with nanoSIMS ^{13}C-stable-isotope labelling [33] revealed both light-driven and dark
102 carbon fixation of PSB. Thereby it was found, that the population of PSB isolate "*Thiodictyon*
103 *syntrophicum*" sp. nov. str. Cad16^T (str. Cad16^T, thereafter) [34] assimilated 26% of the total
104 carbon the chemocline during dark and light incubations [31]. Alternatively, the relative
105 contribution of different PSB and GSB spp. to total carbon assimilation normalized to
106 biomass during daytime was estimated with stable isotope analysis for Lake Cadagno.
107 Thereby, str. Cad16^T only photosynthetically fixed 1.3 to 2 % of the carbon, as estimated from
108 the daily bulk δ^{13}C-mass balance [35].

109 Additional insight came from an *in vitro* quantitative proteomics study with str. Cad16^T
110 growing anaerobically under light and dark with 1 mM H$_2$S [36]. Photosynthesis-driven
111 growth of str. Cad16^T resulted in the relative >1.5× expression of 22 proteins. Most notably,
112 the poly(R)-hydroxyalkanoicacid synthase subunit PhaE and the phasin (PhaP) involved in
113 the synthesis of PHB were found. In contrast, among the 17 proteins overexpressed under
114 dark conditions, three enzymes of the dicarboxylate/4-hydroxybutyrate (DC/HB) cycle were
115 detected, indicating dark carbon fixation through this typically *archeal* pathway.

116 The complete genome of str. Cad16^T gave evidence of the biological functions encoded [37].
117 Similar to *Allochromatium* spp. or *Lamprocystis* spp., str. Cad16^T expresses a type II (quinone
118 type) RC, the membrane-bound protein cascade of cyclic electron transport to generate ATP
119 and reverse electron transport to produce NAD(P)H, and also contains a *cbb*3 type
120 cytochrome *c*. The later may enable microaerobic growth and Fe(III) oxidation of str. Cad16^T
121 [38]. However, no genetic evidence for the possible syntrophic relationship within aggregates
122 of *Desulfocapsa* sp., and also only incomplete Sox and no thiosulfate dehydrogenase Tsd
123 proteins, responsible for SO$_3^{2-}$ oxidation, as previously described for str. Cad16^T by Peduzzi
124 and colleagues [34], were found.

125 With this study, we aimed at elucidating the metabolic pathways of PSB str. Cad16[T] in more

126 detail, to better understand the key metabolic mechanisms involved. The main objectives of

127 this study were: (i) to study differences between day and night in the metabolism of PSB str.

128 Cad16[T] *in situ* at the chemocline of Lake Cadagno and (ii) to monitor the environmental

129 factors longitudinally that determine the metabolic activity of the chemocline community. We

130 used a combination of CO_2 assimilation analysis using ^{14}C-scintillation and proteomics using

131 label-free quantitation tandem mass spectrometry (LFQ-MS[2]) to quantify metabolic activity

132 and the pathways involved in str. Cad16[T]. Relative light intensity and temperature at the depth

133 of the chemocline were measured constantly and several CTD profiles were taken during the

134 incubation. The carbon assimilation rates and protein profiles obtained, thereby revealed a

135 mixotrophic metabolism of str. Cad16[T] influenced by the unique microaerobic *in situ*

136 conditions encountered in summer 2017.

137 .

138

139 3. MATERIALS AND METHODS

140 3.1. Study Site and Field Measurements

141

142 The *in situ* incubations were performed in Lake Cadagno between 13 July 2017 to 23

143 September 2017 with dialysis bags attached to a mooring (46°,33',05,1" N/8°,42',43,0" E,

144 max. depth 18 m) (**suppl. Figure S 1b and c**). From 13 July to 13 September 2017 different physical

145 and chemical parameters were measured alongside the incubations in order to monitor the *in*

146 *situ* chemocline conditions and adjust the incubation depth, if necessary. A CTD

147 (Conductivity, Temperature, Depth) 115 probe (Sea & Sun Technology GmbH, Germany)

148 equipped with temperature, salinity, oxygen, redox potential, chlorophyll *a* (Chl *a*) and

149 turbidity sensors was used to measure physicochemical profiles. Profiles from 13 July 2017

150 were taken as an estimate of chemocline depth (**suppl. Figure S2** HOBO UA-002-64 Pendant data

151 loggers (Onset Computer Corporation, MA, USA) measured relative light (Lux; 180–1'200

152 nm) and temperature at 60 min intervals. Two sensors were placed near the surface (0.05 m

153 depth) and other pairs were positioned 0.4 m apart at the upper and lower part of the rig,

154 respectively (**suppl. Figure S 1c**). An empirical conversion factor of Lux = 0.018 PAR and 0.016

155   PAR (μmol m^{-2} s^{-1}) was used for the surface and below the water, respectively as in ref. [39].

156   The passive HOBO logger values were analyzed after retrieval at the end of the experiment.

157   We additionally had access to CTD data from a parallel project form Dr. Oscar Sepúlveda

158   Steiner and colleagues from EAWAG (Dübendorf, Switzerland) where two CTD profiles

159   were taken daily.

160

3.2. Flow Cytometry for Cell Counting

161

162

163   Flow-cytometry based cell counting was performed as in Danza and colleagues [40]. In short,

164   phototrophic bacteria were identified using 50 μl sub-samples in triplicates with a BD Accuri

165   C6 cytometer (Becton Dickinson, San José, CA, USA). A forward scatter threshold of FSC-H

166   10'000 was applied to exclude abiotic particles. A second red fluorescent (FL3-A) threshold

167   above 1'100 was applied to select for cells emitting autofluorescence due to Chl and BChl.

168   The flow rate was set to 66 μl min^{-1}.

169

3.3. Estimates of Biovolume and Biomass of Bacterial Cells

170

171

172   The biovolume was calculated for strain Cad16^T assuming a median diameter of 2 μm (range;

173   1.4–2.4 μm) for a spherical cell. Biomass was estimated using the conversion factor

174   determined for Lake Cadagno PSB strains 4.5 fmol C m^{-3} [33].

175

3.4. Estimates of Carbon Uptake Rates

176

177

178   We took the estimate from Camacho *et al.* [30] that half of the carbon is fixed through

179   oxygenic and anoxygenic photosynthesis, respectively. Musat and colleagues estimated

180   anoxygenic carbon assimilation for PSB *C. okenii* and GSB *C. clathratiforme* to be 70% and

181   15% of the total daily CO_2 assimilation, respectively [33]. We therefore calculated the uptake

182   rates for the three populations as follows (Eq. 1) where A_{day} is the total uptake rate per cell of

183   the phototrophic community and *F* the fraction as estimated in [33]:

184

185                         $$A_{cyano} = A_{day} \times 0.5 \times F \qquad (1)$$

-**6**-

186

3.5. Bacterial Pure Cultures and Media

188

189 Str. Cad16^T was isolated in 2003 [41] and was subsequently grown in pure culture on

190 Autotrophic Pfennig's medium II [42] at the Laboratory of Applied Microbiology in

191 Bellinzona, Switzerland (LMA) (**Figure S 1a**). The medium contained 0.25 g of KH_2PO_4 l^{-1}, 0.34

192 g of NH_4Cl l^{-1}, 0.5 g of $MgSO_4·7H_2O$ l^{-1}, 0.25 g of $CaCl_2·H_2O$ l^{-1}, 0.34 g of KCl L^{-1}, 1.5 g of

193 $NaHCO_3$ l^{-1}, 0.02 mg of vitamin B12 l^{-1} and 0.5 ml of trace element solution SL12 l^{-1}. The

194 medium was autoclaved under a 80% N_2 / 20% CO_2 atmosphere [43] and 1.1 mM $Na_2S·9H_2O$

195 was added aseptically. The pH was adjusted to 7.0. Cultures were grown in 500 ml glass

196 bottles at ambient temperature and under a 12/12 h light/dark-regime with a 60 W

197 incandescent lamp (6 μ mol quanta m^{-1} s^{-1}). Cells were grown up to a concentration of around

198 3×10^6 cells ml^{-1}. Cell concentrations repeatedly were measured by flow cytometry.

199

200 Cellulose dialysis bags with a 14 kDa cutoff (D9777-100FT, Sigma-Aldrich, Buchs, CH)

201 were rinsed for 1.5 h in Na_2CO_3 (40 g l^{-1}) and 0.01 M EDTA at 60 °C wile stirring. The bags

202 were cleaned with ddH_2O, cut into 0.6 m long pieces, closed by a knot on one end and

203 autoclaved for 20 min at 121 °C. On site, about 80 ml of bacteria culture were filled randomly

204 in each bag, which was closed, attached to a rig and installed in the chemocline within 30 min

205 (**suppl. Figure S 1b**). In total 18 dialysis bags where placed at 12 m depth from 13 July to 23

206 August 2017 and then lowered to 14 m for the remaining campaign.

207

3.6. ^{14}C-Incubations

209

210 The scintillation experiment was performed as in Storelli *et al.* [31]. In short, subsamples

211 from three dialysis bags were pooled together randomly, 7 ml NaH^{14}CO$_3$ (NaH^{14}CO$_3$; 1.0

212 mCi; 8.40 mCi mmol^{-1}, 20 μCi ml^{-1}; Cat. No. NEC-086S Perkin-Elmer, Zurich, Switzerland)

213 were added and incubated in cleaned and autoclaved 50 ml translucent Duran glass bottles

214 (SCHOTT AG, Mainz, Germany). Six replicates of str. Cad16^T cultures were incubated for 4

215 hours during day (1:00–4:00 pm) and night (9:00 pm–12:00 am), respectively. Chemocline

216 background fixation rates were determined in 50 ml chemocline samples. Filtered chemocline

217 lake water (0.45 μm) was used as negative control. Upon retrieval, the amount of β-activity

218   (^{14}C) assimilated by microbes during the incubation time was measured in the laboratory

219   following standard method that included acidification and bubbling of the samples [44].

220

221   The inorganic dissolved carbon concentration was determined with the CaCO$_3$ *Merck*

222   *Spectroquant* kit No. 1.01758.0001 and the *Merck spectroquant Pharo 100* photospectrometer

223   (Merck & Cie, Schaffhausen, Switzerland). Samples were taken at 14 m depth, filtered with

224   0.45 μm filters, pH was tested with indicator paper (MColorpHast, Merck KGaA, Germany)

225   to lie within 6.8–7.0 and triplicate samples were measured.

226

227   Scintillation was done on a *Guardian 1414* liquid scintillation counter (Perkin Elmer Wallac,

228   MA, USA) running with the WinSpectral v.1.40 software. Raw data was statistically analyzed

229   using *t*-tests in Excel (Microsoft Office 2010, v-.14.0.7168.5000).

230

3.7. Protein Extraction and Digest

232

233   Subsamples were transferred to 50 ml tubes upon retrieval and stored at 4 °C in the dark.

234   They were then brought to the lab within 30 min and centrifuged 10'000 *g* at 4 °C for 10 min.

235   The supernatant was discarded and the pellets were re-suspended in 1× PBS pH 7.0 and 1%

236   EDTA-free Protease Inhibitor Cocktail (*v/v*; Thermo Fisher Scientific, Rheinach, Switzerland)

237   and frozen at -20 °C until further processing.

238

239   The cells were thawed, lysed in 5% SDC (w/w) in 100 mM ammonium-bicarbonate buffer

240   containing 1% EDTA-free Protease Inhibitor Cocktail (*v/v*; Thermo Fisher Scientific,

241   Rheinach, Switzerland) and sonicated for 15 min at 200 W at 10 °C with a Bioruptor

242   ultrasonicator (Diagenode SA, Belgium). Samples were then shipped to the Functional

243   Genomic Center Zurich (FGCZ) on dry ice for further processing. Protein concentration was

244   estimated using the Qubit Protein Assay Kit (Thermo Fisher Scientific, Rheinach,

245   Switzerland). The samples were then prepared using a commercial iST Kit (PreOmics,

246   Germany [45]) with an updated version of the protocol. Briefly, 50 μg of protein were

247   solubilized in 'lyse' buffer, boiled at 95 °C for 10 min and processed with High Intensity

248   Focused Ultrasound (HIFU) for 30 s setting the ultrasonic amplitude to 85%. Then the

249   samples were transferred to a cartridge and digested by adding 50 μl of the 'Digest' solution.

250   After incubation (60 min, 37 °C) the digestion was stopped with 100 μl of Stop solution. The

251   solutions in the cartridge were removed by centrifugation at 3'800 *g*, while the peptides were

252   retained by the iST-filter. Finally the peptides were washed, eluted, dried and re-solubilized in

253   'LC-Load' buffer for Tandem Mass spectrometry (MS^2)-analysis.

254

255   ## 3.8. Liquid Chromatography and MS^2-Analysis

256

257   MS^2 analysis was performed on a *QExactive* mass spectrometer coupled to a nano *EasyLC*

258   *1000* HPLC (Thermo Fisher Scientific, Rheinach, Switzerland). Initial solvent composition

259   was 0.1% formic acid for channel A and 0.1% formic acid, 99.9% acetonitrile for channel B,

260   respectively. For each sample 4 μL of peptides were loaded on a commercial Acclaim

261   *PepMap* Trap Column (75 μm × 20 mm; Thermo Fisher Scientific, Rheinach, Switzerland)

262   followed by a *PepMap RSLC* C18 Snail Column (75 μm × 500 mm; Thermo Fisher Scientific,

263   Rheinach, Switzerland). The peptides were eluted at a flow rate of 300 nl min^{-1} by a gradient

264   from 5 to 22% B in 79 min, 32% B in 11 min and 95% B in 10 min. Samples were acquired in

265   a randomized order. The mass spectrometer was operated in data-dependent mode (DDA),

266   acquiring a full-scan MS spectra (300−1'700 *m/z*) at a resolution of 70'000 at 200 *m/z* after

267   accumulation to a target value of 3'000'000, followed by HCD (higher-energy collision

268   dissociation) fragmentation on the twelve most intense signals per cycle. HCD spectra were

269   acquired at a resolution of 35'000, using a normalized collision energy of 25 a. u. and a

270   maximum injection time of 120 ms. The automatic gain control (AGC) was set to 50'000

271   ions. Charge state screening was enabled and singly and unassigned charge states were

272   rejected. Only precursors with intensity above 8'300 were selected for MS^2 (2% underfill

273   ratio). Precursor masses previously selected for MS^2 measurement were excluded from further

274   selection for 30 s, and the exclusion window was set at 10 ppm. The samples were acquired

275   using internal lock mass calibration on *m/z* 371.101 and 445.120.

276

277   ## 3.9. Protein Identification and Label Free Protein Quantification

278

279   The acquired raw MS^2 data were processed by MaxQuant v.1.4.1.2, followed by protein

280   identification using the integrated Andromeda search engine. Each file was kept separate in

281   the experimental design to obtain individual quantitative values. Spectra were searched

282   against a forward str. Cad16^T database (6'237 coding genes), concatenated to a reversed

283 decoyed *fasta* database and common protein contaminants (NCBI Assembly No.
284 ASM281377v1; release date: 2017/12/07). Carbamidomethylation of cysteine was set as fixed
285 modification, while methionine oxidation and N-terminal protein acetylation were set as
286 variable. Enzyme specificity was set to trypsin/P allowing a minimal peptide length of 7
287 amino acids and a maximum of two missed-cleavages. Precursor and fragment tolerance was
288 set to 10 ppm and 0.05 Da for the initial search, respectively. The maximum false discovery
289 rate (FDR) was set to 0.01 for peptides and 0.05 for proteins. Label free quantification was
290 enabled and a 2-min window for match between runs was applied. The re-quantify option was
291 selected. For protein abundance, the intensity (Intensity) as expressed in the protein groups
292 file was used, corresponding to the sum of the precursor intensities of all identified peptides
293 for the respective protein group. Only quantifiable proteins (defined as protein groups
294 showing two or more razor peptides) were considered for subsequent analyses. Protein
295 expression data were transformed (hyperbolic arcsine transformation) and missing values
296 (zeros) were imputed using the *missForest R*-package v.1.4 [46] The protein intensities were
297 normalized by scaling the median protein intensity in each sample to the same values.

298

299 Scaffold v.4.8.4 (Proteome Software Inc., Portland, OR) was used to validate MS^2 based
300 peptide and protein identifications. Peptide identifications were accepted if they could be
301 established at greater than 42.0% probability to achieve an FDR less than 0.1% by the Peptide
302 Prophet algorithm with *Scaffold* [47] delta-mass correction. Protein identifications were
303 accepted if they could be established at greater than 54.0% probability to achieve an FDR less
304 than 1.0% and contained at least two identified peptides. Protein probabilities were assigned
305 by the *Prophet* algorithm [48]. Proteins that contained similar peptides and could not be
306 differentiated based on MS^2 analysis alone were grouped to satisfy the principles of
307 parsimony. Proteins sharing significant peptide evidence were grouped into clusters. For the
308 two-group analysis the statistical testing was performed using (paired) *t*-test on transformed
309 protein intensities (hyperbolic arcsine transformation). Proteins were called significantly
310 differentially expressed if linear fold-change exceeded 2-fold and the *q*-value from the *t*-test
311 was below 0.01.
312 As an alternative method to find differentially expressed proteins, we used the correlation
313 adjusted *t*-Score algorithm provided by the *R*-package sda v.1.3.7 [49] to further analyze the
314 dataset of 1'333 proteins identified with MaxQuant.

315

-**10**-

316 ## 3.10. Protein Functional Annotation

317

318 BlastKOALA v.2.1 [50] and eggNOG v.4.5.1 [51] were used to classify the proteins into

319 functional categories. The complete KEGG-dataset for str. Cad16^T can be found under Ref.

320 [52].

321

322 ## 3.11. Genomic Data Availability

323

324 The complete genome of str. Cad16^T [52] is available under the GenBank assembly

325 GCA_002813775.1.

326

327 ## 3.12. Proteomic Data Availability

328

329 The complete proteomic data of str. Cad16^T have been deposited to the ProteomeXchange

330 Consortium [53] via the PRIDE partner repository [54] under the accession PXD010641 and

331 project DOI 10.6019/PXD010641

332

333 ## 4. RESULTS

334

335 ## 4.1. Physicochemical Parameters from July to August 2017

336

337 Fluctuations in light intensity were positively correlated with the predicted surface radiation

338 and negatively associated with cloud cover, respectively (**suppl. Figure S3 a**). Daily relative

339 average surface light intensity at 12:00 pm was 1'448.9 μmol quanta m^{-2} s^{-1} (4.3–3'769.6)

340 (**suppl. Figure S3 b**). The surface temperature was stable at an average of 15 °C. High temperatures

341 up to 40 °C were measured, due the solar heating of the logger casing (**suppl. Figure S3 b**). The

342 accumulated sunlight were above average for the weeks observed from (**suppl. Figure S4**). From

343 13 July to 23 August 2017 at 12 m depth, an average of 3.7 μmol quanta m^{-2} s^{-1} (0.2–26.2)

-11-

344 was measured. At 12.4 m depth, a mean of 1.3 μmol quanta m^{-2} s^{-1} (0.04–7.8) was registered

345 (**suppl. Figure S3 c and d**). Within this period, changes of turbidity, oxygen and Chl-*a* profiles in the

346 daily CTD profiles indicated that the chemocline had been sinking from 12 to 13–14.5 m

347 depth (**suppl. Figure S5**). To ensure chemocline conditions for the incubations, we adjusted the

348 depth of the rig from 12 to 14 m depth. This resulted in an unexpected reduced relative light

349 intensity at the position of the rig at 14 m for the days 23 August to 13 September 2017. Only

350 an average of 0.4 μmol quanta m^{-2} s^{-1} (0.2–4.0) was measured at 14 m depth from 24 August

351 to 13 September 2017, and no light was measured at 14.4 m depth after 23 August 2017.

352 Temperature was stable around 5 °C (4.6–6.1) at both incubation depths with a positive trend

353 over the months (**suppl. Figure S3 c and d**).

354

4.2. Chemical and Physical Analysis of Lake Cadagno at Sampling Date

356

357 Physicochemical measurements and endpoint-sampling was done on 12 and 13 September

358 2017. The weather was cloudless with weak wind. Two CTD profiles at 1:30 pm and 9:00 pm

359 showed a comparable situation for temperature, dissolved oxygen and conductivity (**Figure 1**).

360 Water temperature was stable at 12 °C from the surface down to the thermocline at 9.5 m,

361 whereas it dropped to 5 °C at 16 m depth at both time points. Dissolved oxygen (DO) was

362 measured at 8.5 mg l^{-1} (265.6 μM) throughout the mixolimnion. From 7 m to 9.5 m depth,

363 DO-concentrations steadily declined to 6 mg l^{-1}, and then more rapidly to 2 mg l^{-1} at 10.5 m

364 depth, at both time points measured. At 14 m depth, 0.4 mg l^{-1} (12.5 μM) and 0.3 mg l^{-1} (9.4

365 μM) were measured during day and night, respectively. Conductivity increased along the

366 profile from 0.13 in the mixolimnion to 0.22 mS cm^{-1} hypolimnion, both at day and night. In

367 contrast, a pronounced turbidity peak (30 FTU) was observed at a depth of 13 m at 1:30 pm

368 whereas a broader distribution of the FTU values (6–16 FTU) from 13 to 14 m depth was

369 observed at 9:00 pm. Water samples taken at 1:30 pm from 14 m depth showed a milky and

370 pink coloration, characteristic for a concentrated PSB community. The total inorganic

371 dissolved carbon concentrations measured at 14 m depth were 1.26 mM at 2:00 pm and 1.46

372 mM 9:00 pm.

373

374

4.3. Microbial Counts and Evaluation

Initial str. Cad16^T cell concentrations were on average 3.1×10^6 cells ml^{-1} in July, as measured by flow cytometry (FCM). The rigged cultures were checked on 23 August 2017 and all dialysis bags were found intact and cells were judged healthy due to the turbid-pinkish appearance. When retrieved for sampling on 12 September 2017, all dialysis bags were still intact, the population was uniformly distributed within the dialysis bags and the cells grew to a mean concentration of 9.3×10^6 cells ml^{-1}. No significant difference in cell concentration and internal complexity was measured between the two sampling groups ($P = 0.74$). In total, the str. Cad16^T cultures grew 3-fold from July to September.

The average cell concentration in the lake sample taken at 14 m was 4.23×10^6 cells ml^{-1} at 1:30 pm, whereas it was 1.69×10^5 cells ml^{-1} at 9:00 pm. However, the later value has to be questioned as the FCM count was below the values obtained for the 0.45 μm filtered lake water of the ^{14}C background control despite that the measured turbidity values were similar (4–5 FTU) at the two time points at 14 m sampling depth (**Figure 1**). FCM revealed that the phototrophic microbial community at 1:30 pm (4.23×10^6 cells ml^{-1}) consists mainly of *C. okenii*, *C. clathratiforme* and cyanobacteria spp. with 1.48×10^6 cells ml^{-1}, 7.45×10^5 cells ml^{-1} and 1.49×10^6 cells ml^{-1}, representing 35, 35 and 17% of the total phototrophic population, respectively.

4.4. *In situ* Carbon Fixation Rates

Absolute carbon fixation rates at the chemocline were comparable between day and night when tested, with medians of 757 nM h^{-1} and 587 nM h^{-1}, respectively (**Figure 2**). Cad16^T fixed carbon in both conditions of light or dark (**Figure 3**). For str. Cad16^T ^{14}C-bicarbonate median uptake rates normalized per cell were significantly different between the conditions with 1'074 amol C cell^{-1} h^{-1} (range: 937–1'585) during the day, and 834 amol C cell^{-1} h^{-1} (range; 650–969) during the night (**Figure 3**). When the uptake rates were normalized to average biovolume (3.6 μm^3 cell^{-1}), 316 amol C μm^{-3} h^{-1} in light and 230 amol C μm^{-3} h^{-1} in the dark were obtained, and a carbon-based doubling time range of 5 to 23 h was calculated for str. Cad16^T. For the dominant phototrophic populations of the chemocline we estimated uptake

-13-

407   rates in amol C cell^{-1} h^{-1} only at day because of uncertain FCM values at night. Thereby PSB

408   *C. okenii*, GSB *Chlorobium* spp. and cyanobacteria assimilated in average 173.35, 73.70 and

409   245.68 amol cell^{-1} h^{-1}, respectively.

410

411   4.5. Total Proteins identified with LC-MS^2-LFQ

412

413   A total of 11 samples, five samples for category 'light' and six samples for category 'dark',

414   were processed and protein quantification was performed using the MaxQuant package. We

415   used corrected *t*-test based statistics in order to identify and quantify proteins. The samples

416   Cad16T_dia_7 ('light') and Cad16T_dia_12 ('dark') were identified as outliers in cluster

417   analysis and were excluded from further data analysis. Therefore, the data analysis was made

418   with four samples of the category 'light' and five samples of the category 'dark'. Overall a

419   total of 1'333 proteins (21% of the total coding CDS) with at least two peptides were

420   identified.

421

422   4.6. Proteins Quantified with LC-MS^2-LFQ

423

424   Peptide identifications were accepted if they could be established at >42.0% probability to

425   achieve an FDR less than 0.1% with Scaffold delta-mass correction, resulting in 12'576

426   spectra included. Protein identifications were accepted if they could be established at >54.0%

427   probability to achieve an FDR less than 1.0% and contained at least two identified peptides.

428   The number of quantified proteins per condition was similar, with an average of 374 for "day"

429   and 354 for "night", respectively. Between 102 and 663 proteins were quantified in each

430   biological replicate (7.2–37% of all IDs). Consequently, 684 proteins were quantified over all

431   samples. Thereof, 21 contaminants were excluded. The remaining 663 CDS were classified

432   with blastKOALA and EggNOG, with 627 annotated CDS for (99%) COG and 460 annotated

433   CDS (69.4%) for blastKOALA, respectively.

434

435   As expected, many of the proteins with unchanged abundance belonged to the functional

436   categories energy conversion, genetic information processing, carbohydrate and amino

437   metabolism and protein modification (**Table 1**). Among the most abundant proteins detected

438   were F$_0$F$_1$ ATPase subunits (AUB84561.1, AUB81565.1, AUB81565.1 and AUB84563.1)

-14-

439   and chaperons (GroEL; AUB81575.1, AUB80010.1, AUB84066.1, DnaK; AUB84026.1).

440   Since cell growth depends on protein synthesis, we found 36 ribosomal subunits as well as

441   elongation factor Tu (AUB80476.1) to be equally abundant.

442   The cells always contained the established components of the dissimilatory sulfate reduction

443   pathway such as ATP-sulfurylase Sat (AUB82369.1), the adenylylsulfate reductase AprAB

444   (AUB82371.1, AUB82370.1) and the sulfite reductase Dsr complex (AUB83448.1–

445   AUB83455.1). A Sqr sulfide:quinone reductase and a glutathione amide reductase GarA

446   homolog to *A. vinosum* putatively involved in intracellular sulfur shuttling [55] were also

447   present. In PSB, sulfur oxidation provides the electrons for cyclic electron transport driven by

448   light. Consequently, in str. Cad16^T PufMCL (AUB85378.1–AUB85380.1) and PuhA

449   (AUB85431.1) subunits forming the RC II and six different PufAB antenna proteins

450   (AUB85355.1–AUB85357.1, AUB85363.1, AUB85361.1, AUB85710.1) were expressed.

451   Additionally we found enzymes for BChl synthesis, terpenoid backbone biosynthesis and

452   carotenoid synthesis. Noteworthy, elements of the reduction pathways driven by

453   photosynthesis are shared with oxidative phosphorylation in PSB. We found in total 23

454   protein subunits involved in substrate respiration including the NADH dehydrogenase

455   subunits NuoCDEFG an HoxFU, the cytochrome reductase CytB and Cyt1, seven F-type

456   ATPase subunits and two *cbb*3 cytochrome *c* oxidase subunits. PSB use the ATP and

457   NAD(P)H derived from photosynthesis to fix CO_2 through the CBB cycle. For str. Cad16^T a

458   complete CBB cycle with the key enzymes CbbM/RbcL RuBisCO form II (AUB81831.1) and

459   phosphoribulokinase PrkB (AUB79979.1) were present. The fixed carbon enters the central

460   carbon metabolism as 3-phospho-D-glycerate. In both growth conditions, str. Cad16^T contains

461   enzymes for glycolysis and gluconeogenesis, as well as pyruvate oxidation, the glyoxylate

462   cycle and the citrate cycle (TCA cycle) in unvaried abundance. Additionally, the presence of

463   malic enzyme (MaeB; AUB82893.1) may allow the entry of malate into the central carbon

464   pathway via pyruvate, is shown for *A. vinosum*. In both conditions examined, the PHB

465   synthase subunits PhaC and PhaE are expressed (AUB80707.1 and AUB84676.1). Also

466   enzymes necessary for amino acid biosynthesis and Co-factor and vitamin synthesis were

467   expressed under both groups analyzed.

468   In a second step, we analyzed the proteome data for significant changes between growth

469   conditions. However, we found a large within-group variation and no proteins were

470   significantly differently expressed between the two growth conditions using (paired) corrected

471   *t*-test on transformed protein intensities (q.mod <0.01).

472

-15-

4.7. Proteins Differentially Expressed

The expression dataset was alternatively analyzed using correlation-adjusted t-scores (CAT scores) in order to additionally address the correlative structure of the dataset as only 4.5% of the proteins are differentially expressed. Thereby, 60 proteins were found differentially expressed (1% of all coding CDS) at a local false discovery rate of lfdr<0.05. (**Table 3**)

During the 'day' period 21 CDS were found relatively more abundant for str. Cad16^T. Thereof, all CDS were annotated with eggNOG (**Table 2**). Growing in the light, str. Cad16^T over-expressed four proteins involved in oxidative phosphorylation that were subunits of NADH:quinone oxidoreductase, cytochrome bc1 complex respiratory unit and AtpC subunit of F-type ATPase. Two enzyme involved in the central carbon pathway were abundant, the glycogen synthase GlgA and the glucose-6-phosphate isomerase GPI involved in glycolysis. The enzyme acetolactate synthase I/III small subunit associated with thiamine synthesis and the A 7,8-dihydroneopterin aldolase FolB involved in tetrahydrofolate biosynthesis were additionally found. Also membrane transport systems were found, including the ABC-2 type transport system and Twin-arginine translocation (Tat). Additionally, chaperone-type proteins DnaJ and proteolytic ClpX were also over-expressed.

Under the condition 'night' 39 proteins were shown to be more abundant and thereof 35 entries (89%) were COG annotated (**Table 3**). Analysis of this data suggested that the NAD(P)H isocitrate dehydrogenase Idh1 responsible first carbon oxidation from oxaloacetate to 2-oxoglutarate in the TCA cycle as well as a FabH 3-oxoacyl-[acyl-carrier-protein] synthase III involved in fatty acid biosynthesis initiation and elongation were abundant. The adenylylsulfate reductase subunit alpha was found, and AprA is responsible for sulfite oxidation to 5'-adenylyl sulfate [56]. Cad16^T further expressed proteins associated to cell division (FtsZ), cell wall formation CpxP, Lysine and branched amino acid synthesis and nucleotide metabolism (Ppx-GppA; exopolyphosphatase and RutE; 3-hydroxypropanoate dehydrogenase). Elements of two secretion pathways were identified, a putative polar amino acid transport system and type II general secretion system. Additional three proteins detected to be more abundant in the dark are involved in stress response. The BolA-family transcriptional regulators, is a general stress-responsive regulator. Rubrerythrin may provide oxidative stress protection via catalytic reduction of intracellular hydrogen peroxide and a ATP-dependent serine protease mediates the degradation of proteins and transitory regulatory proteins, and thereby ensures cell homeostasis

506 ## 5. DISCUSSION

507

508 We compared light to dark carbon fixation metabolism of PSB str. Cad16^T through a
509 combination longitudinal monitoring of physicochemical condition of the Lake
510 Cadagno chemocline, scintillation and quantitative proteomics of cultures incubated *in*
511 *situ*.

512

513 ### 5.1. Monitoring Data

514

515 During the incubation experiment from July to September 2017 the chemocline was
516 actively monitored with CTD and light and temperature profiles were measured
517 passively. This detailed record allowed us to understand the prevailing physicochemical
518 conditions experienced by the str. Cad16^T cultures. Thereby, the average light
519 availability measured was $10\times$ lower than previously recorded at the chemocline,
520 whereas the available DIC concentration was comparable to 2013 [31]. CTD
521 measurements (this study) and FCM counts of the chemocline throughout the summer
522 2017 [57] revealed dense PSB and GSB populations (10^6 cells ml^{-1}) and an additional
523 cyanobacterial bloom down to the monimolimnion from July 2017 on [40] that probably
524 resulted in increased self-shading below a depth of 13 to 14 m [57]. As a consequence,
525 the maximal peak of turbidity related to the PSOB sunk from around 12 to around 14 m
526 depth. For this reason, we decided to hang the dialysis bags lower from 12 to 14 m at
527 the 23 August 2017. The resulting low light conditions at 14 m depth possibly reduced
528 net photosynthesis and subsequent carbon storage capacity and growth for str. Cad16^T
529 as previously observed for PSB *Chromatium* spp. in the Lakes Cisó and Vilar [58, 59].
530 Whereas the monimolimnion has been typically described as anoxic [28], recurrent
531 blooms of oxygenic plankton [30, 57] and optode-based measurements of dissolved
532 oxygen has revealed micro-oxic conditions below 20 nM at the chemocline [60]. Our
533 study helps to understand the consequences of these conditions for the PSOB.

534

5.2. Carbon Uptake Rates

Measured chemocline CO_2-fixation rates at both conditions were within the ranges previously obtained for Lake Cadagno that were between 85 to 8'000 nM h^{-1} with light, and between 27 to 7'608 nM h^{-1} in dark conditions, respectively (**suppl.** Fehler! Verweisquelle konnte nicht gefunden werden.) [30, 33, 61, 31]. Comparable CO_2-assimilation rates have been also measured in other stratified sulfureta as in Spanish karstic lakes with up to 3'000 nM h^{-1} both in light or dark conditions [62].Importantly, it was estimated that only half of the bulk carbon is fixed by anoxygenic photosynthesis in the Lake Cadagno chemocline [30]. Thereof, PSB *C. okenii* is responsible for 70% of the total anoxygenic phototrophic CO_2 assimilation [33] and the concentration was 10^6 cells ml^{-1}—equal to 35% of the total phototrophic microbes— at 14 m depth in this study. Taken together, *C okenii* may have accounted for an average 173.35 amol C $cell^{-1}$ h^{-1} in light conditions in our study, which is 60-fold lower that previously observed [33]. The average GSB assimilation rate with 73.7 amol C $cell^{-1}$ h^{-1} was higher than observed (1–30), but within the same magnitude [33]. Oxygenic photosynthesis contributed 245.68 amol C $cell^{-1}$ h^{-1} to the C-fixation that is 10–100 less than observed in the Baltic sea [63].

For str. Cad16[T], the median uptake rate of 1'073.9 amol C $cell^{-1}$ h^{-1} during the day was within the range measured for other PSB (100–30'000 amol C $cell^{-1}$ h^{-1}) [33, 31], however 10× lower compared to a previous *in situ* ^{14}C-assimilation study with strain Cad16[T] (around 12'000 amol C $cell^{-1}$ h^{-1}) [31]. In the former experiment, autotrophic CO_2 assimilation rates of str. Cad16[T] were additionally measured *in vitro*, with values between 8'541.7–18'541.7 amol C $cell^{-1}$ h^{-1} with light, and around 2'916.7 amol C $cell^{-1}$ h^{-1} in the dark, respectively. For C-fixation at night, highly variable C-assimilation rates in chemocline bulk samples were measured, ranging from 7–45% of the rates measured with light [24]. Schanz and colleagues thereby found a positive correlation between photosynthetically driven increase in overall biomass and dark fixation rates [24]. In our study, the median dark fixation rate of 834.4 amol C $cell^{-1}$ h^{-1} was significantly lower than during the day, and again around 10× lower than measured by Storelli and colleagues [31]. This overall discrepancy may be explained by the 10-fold lower light availability that possibly reduced photosynthetic carbon assimilation and carbon storage (see above). Furthermore the sampling times in our study were adapted to the natural

568   light-dark hours. This was in order to account for possible circadian effects, whereas in

569   the former study incubations were performed in parallel at daytime, using clear and

570   opaque sample bottles.

571   The differences between the study results may further be explained with the varied cell

572   counting methodologies. Fluorescent *in situ*-hybridization (FISH) was used to count

573   cells in the study of Storelli *et al.* [31]. Furthermore, we did not control for dead cells in

574   FCM which might have led to a relative overestimation of the str. Cad16[T] cell

575   concentration. Moreover, str. Cad16[T] forms aggregates, and some stuck to the dialysis

576   bags visible as a pinkish residue, possibly reducing the number of planktonic cells for

577   FCM counting.

578

579   When normalized to biomass, the carbon uptake values at light were higher as

580   previously measured for PSB *C. okenii* and *Lamprocystis* sp. [33]. Uptake rates

581   normalized to biovolume depend on the cell volume estimation (i.e. volume depends on

582   r^3) and the conversion factors chosen. We used values previously used in literature (see

583   methods). For str. Cad16[T], the estimated carbon-based doubling time was between 4 and

584   23 h, which is in contrast to previous estimates of 121 h *in vitro* [34], and a median of

585   333.6 h (25th percentile; 196.8 h, 75th percentile; 652.8 h) for the bulk biomass in the

586   chemocline [24]. In contrast, the average doubling time obtained by FCM counting was

587   948.0 h (39.5 d) which is 40× longer than our ^{14}C-uptake based calculations, and 8×

588   longer than *in vitro* [34]. We did not control for the presence and metabolic activity of

589   the syntrophic *Desulfocapsa* sp. nov. str. Cad626 [69] as it was observed that the str.

590   Cad16[T] *in vitro* cultures we used lost the initially co-occurring str. Cad626 after several

591   years under laboratory growth conditions.

592   The significantly higher inorganic C-uptake rate during the day compared to night-time

593   rates suggests active photosynthesis of str. Cad16[T] at low light intensities, as it was

594   described for other PSB [24, 64]. Noteworthy, the presence of up to 3×10^5 ml^{-1}

595   oxygenic phototrophic microbes down to 16 m depth [40] resulted in a partly

596   oxygenated chemocline with around 0.6 mg O_2 l^{-1} (19 μM), as measured with CTD.

597   Consequently, the chemocline waters retained some of the produced oxygen through the

598   night (**Figure 1**). Taken together, str. Cad16[T] may have used the O_2 present as electron

599   acceptor during mixotrophic growth under both conditions. As a consequence, some of

600   the CO_2 assimilated might have been constantly respired with thiosulfate as electron

601   donor as found for *T. roseopersicina* str. M1 [15]. In accordance, str. Cad16[T] grew in

-19-

602   the dark with thiosulfate and 5% O_2 *in vitro* [41]. Interestingly however, we found only

603   SoxXY and SoxB and no TsdA thiosulfate-oxidizing enzyme homologues encoded in

604   the str. Cad16^T genome [52]. As the complete Sox-complex is essential for the complete

605   thiosulfate oxidation to sulfate in *A. vinosum* DSM 180^T [65], str. Cad16^T possibly uses

606   an alternative mechanism. One alternative may be thiosulfate uptake through CysTWA

607   (AUB80378.1, AUB80379.1 and AUB80380.1) and CysP (AUB80377.1) and oxidation

608   to sulfite via the intermediate S-sulfocysteine by cysteine synthase B CysM

609   (AUB82938.1) and possibly monothiol glutaredoxin of the Grx4 family (AUB83488.1)

610   as suggested by Dahl [66]. However, with the applied methods we could not determine

611   the relative contributions of photosynthetic or chemotrophic activity to the total increase

612   in biomass. To conclude, ^{14}C-fixation rates and FCM counting indicated an actively

613   growing str. Cad16^T population during the incubation. The findings on carbon

614   assimilation rates are further reflected in the proteome (discussed below).

615

616   5.3. Stable Fraction of the Strain Cad16^T Proteome

617

618   In order to understand differences in metabolism, the str. Cad16^T light/dark proteome

619   has been studied extensively. Previously, Storelli and colleagues [36] performed a

620   comparable proteomics study on light/dark metabolism, str. Cad16^T *in vitro* with 2D-

621   difference gel electrophoresis (2D-DiGE), where they identified around 1'400 proteins,

622   quantified 56 and, thereof, found 37 differentially expressed proteins. With six

623   biological replicates instead of three, and the increased resolution and high-throughput

624   capacity of LC-MS^{2+} compared to 2D-DiGE [67], we expected to substantially increase

625   protein identification and quantitation in comparison. Overall, the number of identified

626   proteins was comparable in both studies, with 1'400 in Ref [36] to 1'333 in our study.

627   Noteworthy, LC-MS^2 analysis returns sequence information on all proteins identified,

628   whereas 2D-DiGE is limited to a chosen subset, based on the relative intensity and size

629   of the protein spots on the gel. Therefore, we could quantify as much as 663 proteins

630   that are 12× more than in the former study. Nevertheless, the number of unique proteins

631   with different abundance between the two growth conditions was comparable, with 62

632   in our study versus 37 in the former, respectively. Interestingly, we retrieved only 28 of

633   these proteins in the constantly expressed fraction of the proteome.

634   In addition to technical differences, the former study was performed *in vitro* under an

635   anaerobic atmosphere, with higher light intensities (6 μmol m^{-2} s^{-1}) and at 20 °C, which

636   may have an influence on metabolic rates and relative activity. In conclusion, the results

637   of the present study can only be compared to some extend with previous findings.

638

639   The photosynthesis apparatus was abundant in both growth conditions, as several LHC

640   proteins were detected. In accordance, also the enzymatic pathway for BChl*a* and

641   carotenoid synthesis was expressed. In *T. roseopersicina* BChl*a* was absent at

642   prolonged exposure to 60 μM O$_2$ in darkness [68]. In contrast, for str. Cad16^T we did

643   not observe a loss of pigmentation. This might suggest that BChl*a* was not regulated on

644   expression level and/or the micro-oxic conditions did not influence BChl*a* biosynthesis.

645   The central role of dissimilatory sulfur oxidation during photosynthesis is well

646   established for PSB [69] and proteins involved were found expressed in str. Cad16^T.

647   The proteins Sqr, Dsr and Sat were present and SGBs were also observed

648   microscopically in both conditions. The CBB cycle is central in purple bacteria, not

649   only for autotrophic carbon fixation, but also to regenerate the pool of reduced co-

650   factors NAD[P]H$_2$ [70]. Strain Cad16^T contains two forms of RuBisCo, RbcAB form I

651   and RbcSL form II. In a previous study Storelli and colleagues [31] detected

652   constitutive transcription of the *rbcL* gene under autotrophic condition *in vitro* under a

653   12/12 h dark/light regime, whereas the form I *rbcA* was induced by light. In contrast

654   both *rbc* genes were transcribed equally under heterotrophic conditions with acetate,

655   with and without light, respectively [31]. In our study we detected RbcL to be equally

656   abundant in both conditions and no other RuBisCo subunits were found. Therefore, the

657   sole presence of the dimeric form II RuBisCo may underline the importance of CO$_2$

658   fixation mediated by the CBB cycle in maintaining the redox-balance under chemo or

659   mixotrophic growth at low light and dark conditions, as described for purple bacteria

660   [71].

661

662   In str. Cad16^T, the CsrA (AUB84364.1) seems to be the main carbon storage regulator

663   where it was detected under both conditions. Glycolysis under mixotrophic conditions

664   might thereby be regulated through mRNA transcription and stability as in *A. vinosum*

665   [56]. We additionally found enzymes involved in the central carbon pathways TCA,

666   EMP and glyoxylate cycle in unvaried abundance. Noteworthy, isocitrate lyase was

667   found expressed, that is involved in the glyoxylate cycle, that prevents loss of CO$_2$ and

668 ensures production of NAD[P]H$_2$ otherwise occurring through the isocitrate

669 dehydrogenase and 2-oxoglutarate dehydrogenase in the TCA [72]. Further, the malic

670 enzyme was abundant, that generates oxaloacetate via malate through anaplerotic

671 reactions without ATP [73]. The *ccb*3 cytochrome *c* oxidase found in both conditions is

672 used in aerobic respiration and additionally used for FeS oxidation and it was speculated

673 that str. Cad16^T is also involved in both aerobic [38] and anaerobic cryptic iron cycling,

674 as found for *Thiodictyon* str. F4 [74]. Taken together, the metabolic fate of the carbon

675 fixed is only partly elucidated by proteome analysis and metabolic carbon pathways

676 may be active under the conditions examined.

677

678 ## 5.4. Differentially Expressed Proteome

679

680 In light conditions, members of the oxidative respiration pathway were upregulated,

681 indicating an active substrate respiration with light as in *T. roseopersicina* [20].

682 However, the cytochrome *bc* and the NADH-dehydrogenase complex and redox carrier

683 molecules are also used in cyclic electron transport during photosynthesis in PSB.

684 During light conditions, both chemotrophic and phototrophic metabolism compete for

685 electrons in str. Cad16^T. We also found evidence for glycolysis / gluconeogenesis since

686 GPI was overexpressed. Interestingly, the glycogen synthase GlgA was additionally

687 found abundant in the light. Glycogen synthesis and sulfur oxidation was found to be

688 ineffectively regulated in *A. vinosum* [75] and we might speculate that in str. Cad16^T

689 both processes are highly active even at slow growth, allowing for both, intracellular

690 sulfur and glycogen accumulation. Altogether, these results indicate an active

691 phototrophic and chemotrophic metabolism competing for electrons in the light.

692

693 In the dark, the micro-oxic condition may have led to the production of reactive oxygen

694 species in str. Cad16^T that would explain the upregulated proteins involved in stress

695 induced damage-control.

696 Interestingly, AprA was more abundant in the night period, indicating a relative higher

697 activity of sulfite oxidation possibly coupled to chemotrophy. SGBs are consumed

698 under dark autotrophic conditions in PSB *C. okenii* and *C. minus* observed *in vitro* [12],

699 however the side scatter values measured did not vary between the two sample groups

700 in this study when monitored with FCM. This may be due to glycogen and PHB storage

701 inclusions, structures that add up additional structural complexity and de-
702 polymerization kinetics may be different to those of SGB. Supporting evidence is given
703 by the unchanged presence of enzymes involved in of glycogen and PSB synthesis.
704
705 In summary, the 60 proteins found differentially expressed represent only about 1% of
706 all protein coding CDS and about 5% of the identified proteins. Therefore, their impact
707 on metabolic pathways is unclear and has to be further examined

708 ## 6. CONCLUSION AND OUTLOOK

709

710 PSB str. Cad 16^T is metabolically flexible and growths phototrophically as well as
711 chemotropically in the light as shown in this study. In dark conditions, low levels of
712 oxygen may enable respiration of different small organic molecules. In order to
713 understand the dark carbon metabolism, uptake experiments with labelled acetate and or
714 pyruvate should be therefore included in the future. The long-term observation of the
715 chemocline revealed the relative importance of oxygenic phototrophs on the
716 oxygenation of the chemocline. However, it is not clear if O_2 or reduced sulfur is used
717 as terminal electron acceptor in str. Cad16^T. Furthermore, the oxidation of Fe(II) to fix
718 CO_2 should be tested for str. Cad16^T *in vitro*, both under microaerobic and anaerobic
719 conditions as found in Lake Cadagno in 2017. To better estimate the relative metabolic
720 contributions of the different phototrophic energy metabolism at microaerobic
721 conditions oxygenic photosynthesis-inhibitors [76] should be included in future
722 experiments as a control. The contribution of phytoplankton to dark carbon uptake [77]
723 has also not yet been elucidated in Lake Cadagno and therefore a sequential size
724 dependent fractionation of sub-samples would be interesting. In order to further
725 understand transcriptional control over the light to dark metabolism also mRNA
726 sequencing experiments would be needed. To complete the understanding metabolomic
727 studies would give insight into the relative amount of metabolic intermediates produced
728 under different regimes. We further observed a large variability in the C-uptake rates
729 between different studies that cannot be readily explained by differences in the
730 chemocline community composition and/or technical variances. Therefore, NanoSIMS
731 experiments [78] on Cad16^T may help to determine the within-population heterogeneity
732 in inorganic C-assimilation under variable growth regimes.

733

7. REFERENCES

1. Falkowski PG, Fenchel T, Delong EF. The Microbial Engines That Drive Earth's Biogeochemical Cycles. Science. 2008;320:1034–9.

2. Hohmann-Marriott M, Blankenship RE. Variable fluorescence in green sulfur bacteria. Biochim Biophys Acta. 2007;1769:106–13.

3. Blankenship RE, Madigan MT, Bauer CE, editors. Anoxygenic Photosynthetic Bacteria. Dordrecht: Springer Netherlands; 1995. http://link.springer.com/10.1007/0-306-47954-0. Accessed 19 Apr 2016.

4. Imhoff JF. The Family Chromatiaceae. In: Rosenberg E, DeLong EF, Lory S, Stackebrandt E, Thompson F, editors. The Prokaryotes. Springer Berlin Heidelberg; 2014. p. 151–78. doi:10.1007/978-3-642-38922-1_295.

5. Pfennig N, Markham MC, Liaaen-Jensen S. Carotenoids of Thiorhodeceae. 8. Isolation and characterization of a Thiothece, Lamprocystis and Thiodictyon strain and their carotenoid pigments. Arch Für Mikrobiol. 1968;62:178–91.

6. Wagner-Huber R, Brunisholz RA, Bissig I, Frank G, Suter F, Zuber H. The primary structure of the antenna polypeptides of Ectothiorhodospira halochloris and Ectothiorhodospira halophila. Four core-type antenna polypeptides in E. halochloris and E. halophila. Eur J Biochem FEBS. 1992;205:917–25.

7. Weissgerber T, Zigann R, Bruce D, Chang Y-J, Detter JC, Han C, et al. Complete genome sequence of Allochromatium vinosum DSM 180(T). Stand Genomic Sci. 2011;5:311–30.

8. Tabita FR. Molecular and Cellular Regulation of Autotrophic Carbon Dioxide Fixation in Microorganismst. 1988;:36.

9. Prange A, Dahl C, Truper HG, Behnke M, Hahn J, Modrow H, et al. Investigation of S-H bonds in biologically important compounds by sulfur K-edge X-ray absorption spectroscopy. Eur Phys J D. 2002;20:589–96.

10. Schlegel HG. Die Speicherstoffe von Chromatium okenii. Arch Für Mikrobiol. 1962;42:110–6.

11. Gemerden H van. On the ATP generation by Chromatium in darkness. Arch Microbiol. 1968;64:118–124.

12. Del Don CD, Hanselmann KW, Peduzzi R, Bachofen R. Biomass composition and methods for the determination of metabolic reserve polymers in phototrophic sulfur bacteria. Aquat Sci. 1994;56:1–15.

13. Niel CBV. The Bacterial Photosyntheses and Their Importance for the General Problem of Photosynthesis. In: Advances in Enzymology and Related Areas of Molecular Biology. Wiley-Blackwell; 1941. p. 263–328. doi:10.1002/9780470122464.ch8.

769   14. Bogorov LV. O svoĭstvakh Thiocapsa roseopersicina, shtamm BBS, vydelennogo iz
770   éstuariia Belogo moria. Mikrobiologiia. 1974;43:326–32.

771   15. Wit R de, Gemerden H van. Chemolithotrophic growth of the phototrophic sulfur
772   bacterium Thiocapsa roseopersicina. FEMS Microbiol Ecol. 1987;3:117–26.

773   16. Hurlbert RE. Effect of Oxygen on Viability and Substrate Utilization in Chromatium. J
774   Bacteriol. 1967;93:1346–52.

775   17. Kondratieva EN, Zhukov VG, Ivanovsky RN, Petushkova YP, Monosov EZ. The capacity
776   of phototrophic sulfur bacterium Thiocapsa roseopersicina for chemosynthesis. Arch
777   Microbiol. 1976;108:287–92.

778   18. Kämpf C, Pfennig N. Chemoautotrophic growth of Thiocystis violacea, Chromatium
779   gracile and C. vinosum in the dark at various O2-concentrations. J Basic Microbiol.
780   1986;26:517–31.

781   19. Overmann J, Pfennig N. Continuous chemotrophic growth and respiration of
782   Chromatiaceae species at low oxygen concentrations. Arch Microbiol. 1992;158:59–67.

783   20. Schaub BEM, Gemerden H van. Simultaneous phototrophic and chemotrophic growth in
784   the purple sulfur bacterium Thiocapsa roseopersicina M1. FEMS Microbiol Ecol.
785   1994;13:185–95.

786   21. Rákhely G, Laurinavichene TV, Tsygankov AA, Kovács KL. The role of Hox
787   hydrogenase in the H2 metabolism of Thiocapsa roseopersicina. Biochim Biophys Acta BBA
788   - Bioenerg. 2007;1767:671–6.

789   22. Genovese S, TRÜPER HG. Characterization of Photosynthetic Sulfur Bacteria Causing
790   Red Water in Lake Faro (messina Sicily). Limnol Oceanogr. 1968;13:225 &.

791   23. Sorokin YI. Interrelations between sulphurand carbon turnover in meromictic lakes. Arch
792   Hydrobiol. 1970;66:391–446.

793   24. Schanz F, Fischer-Romero C, Bachofen R. Photosynthetic Production and
794   Photoadaptation of Phototrophic Sulfur Bacteria in Lake Cadagno (Switzerland). Limnol
795   Oceanogr. 1998;43:1262–9.

796   25. Tonolla M, Demarta A, Peduzzi R, Hahn D. In situ analysis of phototrophic sulfur
797   bacteria in the chemocline of meromictic Lake Cadagno (Switzerland). Appl Environ
798   Microbiol. 1999;65:1325–30.

799   26. Hamilton TL, Bovee RJ, Thiel V, Sattin SR, Mohr W, Schaperdoth I, et al. Coupled
800   reductive and oxidative sulfur cycling in the phototrophic plate of a meromictic lake.
801   Geobiology. 2014;12:451–68.

802   27. Pjevac P, Korlević M, Berg JS, Bura-Nakić E, Ciglenečki I, Amann R, et al. Community
803   Shift from Phototrophic to Chemotrophic Sulfide Oxidation following Anoxic Holomixis in a
804   Stratified Seawater Lake. Appl Environ Microbiol. 2015;81:298–308.

805   28. Del Don C, Hanselmann KW, Peduzzi R, Bachofen R. The meromictic alpine Lake
806   Cadagno: orographical and biogeochemical description. Aquat Sci. 2001;63:70–90.

807   29. Tonolla M, Storelli N, Danza F, Ravasi D, Peduzzi S, Posth NR, et al. Lake Cadagno:
808   Microbial Life in Crenogenic Meromixis. In: Gulati RD, Zadereev ES, Degermendzhi AG,
809   editors. Ecology of Meromictic Lakes. Cham: Springer International Publishing; 2017. p.
810   155–86. doi:10.1007/978-3-319-49143-1_7.

811   30. Camacho A, Erez J, Chicote A, Florín M, Squires MM, Lehmann C, et al. Microbial
812   microstratification, inorganic carbon photoassimilation and dark carbon fixation at the
813   chemocline of the meromictic Lake Cadagno (Switzerland) and its relevance to the food web.
814   Aquat Sci. 2001;63:91–106.

815   31. Storelli N, Peduzzi S, Saad MM, Frigaard N-U, Perret X, Tonolla M. CO2 assimilation in
816   the chemocline of Lake Cadagno is dominated by a few types of phototrophic purple sulfur
817   bacteria. FEMS Microbiol Ecol. 2013;84:421–432.

818   32. Casamayor EO, García-Cantizano J, Pedrós-Alió C. Carbon dioxide fixation in the dark
819   by photosynthetic bacteria in sulfide-rich stratified lakes with oxic-anoxic interfaces. Limnol
820   Oceanogr. 2008;53:1193–1203.

821   33. Musat N, Halm H, Winterholler B, Hoppe P, Peduzzi S, Hillion F, et al. A single-cell
822   view on the ecophysiology of anaerobic phototrophic bacteria. Proc Natl Acad Sci U S A.
823   2008;105:17861–6.

824   34. Peduzzi S, Storelli N, Welsh A, Peduzzi R, Hahn D, Perret X, et al. Candidatus
825   "Thiodictyon syntrophicum", sp. nov., a new purple sulfur bacterium isolated from the
826   chemocline of Lake Cadagno forming aggregates and specific associations with Desulfocapsa
827   sp. Syst Appl Microbiol. 2012;35:139–44.

828   35. Posth NR, Bristow LA, Cox RP, Habicht KS, Danza F, Tonolla M, et al. Carbon isotope
829   fractionation by anoxygenic phototrophic bacteria in euxinic Lake Cadagno. Geobiology.
830   2017;15:798–816.

831   36. Storelli N, Saad MM, Frigaard N-U, Perret X, Tonolla M. Proteomic analysis of the
832   purple sulfur bacterium Candidatus "Thiodictyon syntrophicum" strain Cad16T isolated from
833   Lake Cadagno. EuPA Open Proteomics. 2014. doi:10.1016/j.euprot.2013.11.010.

834   37. Luedin SM, Pothier JF, Danza F, Storelli N, Frigaard N-U, Wittwer M, et al. Complete
835   genome   sequence   of   "Thiodictyon   syntrophicum"   sp.   nov.   strain   Cad16T,   a
836   photolithoautotrophic purple sulfur bacterium isolated from the alpine meromictic Lake
837   Cadagno. Stand Genomic Sci. 2018.

838   38. Berg JS, Michellod D, Pjevac P, Martinez-Perez C, Buckner CRT, Hach PF, et al.
839   Intensive cryptic microbial iron cycling in the low iron water column of the meromictic Lake
840   Cadagno: A cryptic microbial iron cycle. Environ Microbiol. 2016;18:5288–302.

841   39. Thimijan RW. Photometric, Radiometric, and Quantum Light Units of Measure A Review
842   of Procedures for Interconversion. 1983;18:5.

843   40. Danza F, Storelli N, Roman S, Lüdin S, Tonolla M. Dynamic cellular complexity of
844   anoxygenic phototrophic sulfur bacteria in the chemocline of meromictic Lake Cadagno.
845   PLOS ONE. 2017;12:e0189510.

846   41. Peduzzi S, Tonolla M, Hahn D. Isolation and characterization of aggregate-forming
847   sulfate-reducing and purple sulfur bacteria from the chemocline of meromictic Lake Cadagno,
848   Switzerland. FEMS Microbiol Ecol. 2003;45:29–37.

849   42. Eichler B, Pfennig N. A new purple sulfur bacterium from stratified freshwater lakes,
850   Amoebobacter purpureus sp. nov. Arch Microbiol. 1988;149:395–400.

851   43. Widdel F, Bak F. Gram-Negative Mesophilic Sulfate-Reducing Bacteria. In: The
852   Prokaryotes. Springer, New York, NY; 1992. p. 3352–78. doi:10.1007/978-1-4757-2191-
853   1_21.

854   44. Gächter R, Mares A, Tilzer MM. Determination of phytoplankton production by the
855   radiocarbon method: a comparison between the acidification and bubbling method (ABM)
856   and the filtration techn1que. J Plankton Res. 1984;6:359–64.

857   45. preomics-sample-prep-kit-protocol-cartridge-96x-v_3_0_b.pdf. iST Sample Preparation
858   Kit (96 reactions) PROTOCOL - Pelleted cells & precipitated protein. 2018.
859   http://preomics.com/resources/preomics-sample-prep-kit-protocol-cartridge-96x-v_3_0_b.pdf.
860   Accessed 31 Jul 2018.

861   46. Stekhoven DJ, Bühlmann P. MissForest—non-parametric missing value imputation for
862   mixed-type data. Bioinformatics. 2012;28:112–8.

863   47. Keller A, Nesvizhskii AI, Kolker E, Aebersold R. Empirical Statistical Model To Estimate
864   the Accuracy of Peptide Identifications Made by MS/MS and Database Search. Anal Chem.
865   2002;74:5383–92.

866   48. Nesvizhskii AI, Keller A, Kolker E, Aebersold R. A statistical model for identifying
867   proteins by tandem mass spectrometry. Anal Chem. 2003;75:4646–58.

868   49. Ahdesmäki M, Strimmer K. Feature selection in omics prediction problems using cat
869   scores and false nondiscovery rate control. Ann Appl Stat. 2010;4:503–19.

870   50. Kanehisa M, Sato Y, Morishima K. BlastKOALA and GhostKOALA: KEGG Tools for
871   Functional Characterization of Genome and Metagenome Sequences. J Mol Biol.
872   2016;428:726–31.

873   51. Huerta-Cepas J, Forslund K, Szklarczyk D, Jensen LJ, von Mering C, Bork P. Fast
874   genome-wide functional annotation through orthology assignment by eggNOG-mapper.
875   bioRxiv. 2016;:076331.

876   52. KEGG PATHWAY: Metabolic pathways - Candidatus Thiodictyon syntrophicum.
877   https://www.kegg.jp/kegg-bin/show_pathway?tsy01100. Accessed 1 Jun 2018.

878   53. ProteomeXchange Datasets. http://proteomecentral.proteomexchange.org/cgi/GetDataset.
879   Accessed 4 Jun 2018.

880   54. Vizcaíno JA, Côté RG, Csordas A, Dianes JA, Fabregat A, Foster JM, et al. The
881   Proteomics Identifications (PRIDE) database and associated tools: status in 2013. Nucleic
882   Acids Res. 2012;41:D1063–9.

883   55. Frigaard N-U, Dahl C. Sulfur Metabolism in Phototrophic Sulfur Bacteria. In: Poole RK,
884   editor. Advances in Microbial Physiology. Academic Press; 2008. p. 103–200.

885   http://www.sciencedirect.com/science/article/pii/S0065291108000027. Accessed 16 Mar
886   2016.

887   56. Weissgerber T, Sylvester M, Kröninger L, Dahl C. A Comparative Quantitative Proteomic
888   Study Identifies New Proteins Relevant for Sulfur Oxidation in the Purple Sulfur Bacterium
889   Allochromatium vinosum. Appl Environ Microbiol. 2014;80:2279–92.

890   57. Danza F, Ravasi D, Storelli N, Roman S, Luedin SM, Bueche M, et al. Microbial diversity
891   in the water column of meromictic Lake Cadagno and evidence for seasonal dynamics. 2018.

892   58. Montesinos E, Esteve I. Effect of algal shading on the net growth and production of
893   phototrophic sulfur bacteria in lakes of the Banyoles karstic area. SIL Proc 1922-2010.
894   1984;22:1102–5.

895   59. Guerrero R, Montesinos E, Pedrós-Alió C, Esteve I, Mas J, Van Gemerden H, et al.
896   Phototrophic sulfur bacteria in two Spanish lakes: vertical distribution and limiting factors.
897   Limnol Oceanogr. 1985;30:919–931.

898   60. Milucka J, Kirf M, Lu L, Krupke A, Lam P, Littmann S, et al. Methane oxidation coupled
899   to oxygenic photosynthesis in anoxic waters. ISME J. 2015;9:1991–2002.

900   61. Halm H, Musat N, Lam P, Langlois R, Musat F, Peduzzi S, et al. Co-occurrence of
901   denitrification and nitrogen fixation in a meromictic lake, Lake Cadagno (Switzerland).
902   Environ Microbiol. 2009;11:1945–58.

903   62. Casamayor EO, Llirós M, Picazo A, Barberán A, Borrego CM, Camacho A. Contribution
904   of deep dark fixation processes to overall CO2 incorporation and large vertical changes of
905   microbial populations in stratified karstic lakes. Aquat Sci. 2012;74:61–75.

906   63. Klawonn I, Nahar N, Walve J, Andersson B, Olofsson M, Svedén JB, et al. Cell-specific
907   nitrogen- and carbon-fixation of cyanobacteria in a temperate marine system (Baltic Sea).
908   Environ Microbiol. 18:4596–609.

909   64. Gemerden H van. Survival of Chromatium vinosum at low light intensities. Arch
910   Microbiol. 1980;125:115–21.

911   65. Hensen D, Sperling D, Trüper HG, Brune DC, Dahl C. Thiosulphate oxidation in the
912   phototrophic sulphur bacterium Allochromatium vinosum. Mol Microbiol. 2006;62:794–810.

913   66. Dahl C. Sulfur Metabolism in Phototrophic Bacteria. In: Hallenbeck PC, editor. Modern
914   Topics in the Phototrophic Prokaryotes. Springer International Publishing; 2017. p. 27–66.
915   doi:10.1007/978-3-319-51365-2_2.

916   67. Wöhlbrand L, Trautwein K, Rabus R. Proteomic tools for environmental microbiology—
917   A roadmap from sample preparation to protein identification and quantification.
918   PROTEOMICS. 2013;13:2700–2730.

919   68. Witt R de, Gemerden H van. Growth of the phototrophic purple sulfur bacterium
920   Thiocapsaroseopersicina under oxic/anoxic regimens in the light. FEMS Microbiol Ecol.
921   1990;6:69–76.

922   69. Trüper HG. CO2-Fixierung und Intermediärstoffwechsel bei Chromatium okenii Perty.
923   Arch Für Mikrobiol. 1964;49:23–50.

924 70. McKinlay JB, Harwood CS. Carbon dioxide fixation as a central redox cofactor recycling
925 mechanism in bacteria. Proc Natl Acad Sci. 2010;107:11669–75.

926 71. Laguna R, Joshi GS, Dangel AW, Luther AK, Tabita FR. Integrative control of carbon,
927 nitrogen, hydrogen, and sulfur metabolism: the central role of the Calvin-Benson-Bassham
928 cycle. Adv Exp Med Biol. 2010;675:265–71.

929 72. Kornberg HL. Aspects of Terminal Respiration in Microorganisms. Annu Rev Microbiol.
930 1959;13:49–78.

931 73. Tang K-H, Tang YJ, Blankenship RE. Carbon Metabolic Pathways in Phototrophic
932 Bacteria and Their Broader Evolutionary Implications. Front Microbiol. 2011;2.
933 doi:10.3389/fmicb.2011.00165.

934 74. Croal LR, Johnson CM, Beard BL, Newman DK. Iron isotope fractionation by Fe(II)-
935 oxidizing photoautotrophic bacteria. Geochim Cosmochim Acta. 2004;68:1227–42.

936 75. Beeftink HH, van Gemerden H. Actual and potential rates of substrate oxidation and
937 product formation in continuous cultures ofChromatium vinosum. Arch Microbiol.
938 1979;121:161–7.

939 76. Draber Wilfried, Tietjen Klaus, Kluth Joachim F., Trebst Achim. Herbicides in
940 Photosynthesis Research. Angew Chem Int Ed Engl. 1991;30:1621–33.

941 77. Znachor P, Nedoma J. Importance of dissolved organic carbon for phytoplankton nutrition
942 in a eutrophic reservoir. J Plankton Res. 2010;32:367–76.

943 78. Behrens S, Kappler A, Obst M. Linking environmental processes to the *in situ* functioning
944 of microorganisms by high-resolution secondary ion mass spectrometry (NanoSIMS) and
945 scanning transmission X-ray microscopy (STXM): NanoSIMS and STXM in environmental
946 microbiology. Environ Microbiol. 2012;14:2851–69.

947 79. Zuber V, Strimmer K. Gene ranking and biomarker discovery under correlation.
948 Bioinformatics. 2009;25:2700–7.

949

8. AUTHOR CONTRIBUTIONS

9. ACKNOWLEDGEMENTS

967
968
969
970
971
972
973
974
975
976
977
978
979
980
981
982
983

984 **10. TABLES AND FIGURES**

985 ## 10.1. Tables

986 **Table 1 | Functional categories of "*Thyodictyon syntrophicum*" str. Cad16^T proteins quantified using** EggNOG v.4.5.1 **[50]** and
987 blastKOALA v.2.1 **[50]** was used to classify proteins according to COG and KEGG classification, respectively.

COG Code	Description	No. Entries
J	Translation, ribosomal structure and biogenesis	64
K	Transcription	15
L	Replication, recombination and repair	7
D	Cell cycle control, Cell division, chromosome partitioning	5
V	Defense mechanisms	3
T	Signal transduction mechanisms	19
M	Cell wall/membrane biogenesis	28
N	Cell motility	1
U	Intracellular trafficking and secretion	10
O	Posttranslational modification, protein turnover, chaperones	50
C	Energy production and conversion	93
G	Carbohydrate transport and metabolism	35
E	Amino acid transport and metabolism	52
F	Nucleotide transport and metabolism	12
H	Coenzyme transport and metabolism	27
I	Lipid transport and metabolism	18
P	Inorganic ion transport and metabolism	37
Q	Secondary metabolites biosynthesis, transport and catabolism	6
KEGG Functional Category		
	Genetic information processing	78
	Carbohydrate metabolism	78
	Energy metabolism	41
	Metabolism of cofactors and vitamins	29
	Amino acid metabolism	28
	Environmental information processing	27
	Nucleotide metabolism	17
	Metabolism of terpenoids and polyketides	11
	Lipid metabolism	9
	Metabolism of other amino acids	5

988

989

990

991

992

993

994   **Table 2 | List of "*Thiodictyon syntrophicum*" str. Cad16^T proteins identified as more abundant in the light period.** Lfdr: local
995   false discovery rate, cat: *t*-score for each group and feature the cat score of the centroid versus the pooled mean **[79]**.

| Accession	Name	COG category	cat score	lfdr
AUB81546.1	cytochrome c1	C	5.44	9.53E-11
AUB83791.1	NADH-quinone oxidoreductase subunit I	C	4.35	8.32E-05
AUB84560.1	F0F1 ATP synthase subunit epsilon	C	3.51	2.26E-04
AUB83997.1	acetolactate synthase small subunit	E	2.88	1.23E-02
AUB81260.1	glucose-6-phosphate isomerase	G	3.63	2.26E-04
AUB83261.1	starch synthase	G	4.48	2.53E-06
AUB79823.1	thiazole synthase	H	2.74	2.93E-02
AUB81699.1	dihydroneopterin aldolase	H	3.41	1.29E-03
AUB83078.1	DNA topoisomerase I	L	2.98	3.81E-03
AUB84659.1	outer membrane lipoprotein carrier protein LolA	M	5.43	2.03E-10
AUB82245.1	HflK protein	O	6.34	1.24E-13
AUB82609.1	ATP-dependent protease ATP-binding subunit ClpX	O	3.38	1.29E-03
AUB84025.1	molecular chaperone DnaJ	O	6.17	1.24E-13
AUB79510.1	hypothetical protein	S	2.84	1.23E-02
AUB81403.1	hypothetical protein	S	3.53	2.26E-04
AUB82197.1	hypothetical protein	S	3.54	2.26E-04
AUB82687.1	hypothetical protein	S	3.96	1.21E-04
AUB83592.1	histidine kinase	S	3.51	1.29E-03
AUB84052.1	host attachment protein	S	3.51	2.26E-04
AUB84690.1	hypothetical protein	U	3.02	3.81E-03
AUB80231.1	multidrug ABC transporter ATP-binding protein	V	3.83	1.21E-04

996

997

998 **Table 3 | List of "*Thyodictyon syntrophicum*" str. Cad16^T proteins identified as more abundant in the dark period**. Lfdr: local
999 false discovery rate, cat: *t*-score for each group and feature the cat score of the centroid versus the pooled mean **[79]**.
1000

| Accession	Name	COG category	cat score	lfdr
AUB80187.1	isocitrate dehydrogenase (NADP)	C	2.94	3.81E-03
AUB81294.1	oxidoreductase	C	3.54	2.26E-04
AUB82371.1	adenylylsulfate reductase alpha subunit	C	3.03	3.81E-03
AUB83156.1	NADH dehydrogenase NAD(P)H nitroreductase	C	3.03	3.81E-03
AUB84003.1	rubrerythrin	C	2.54	4.44E-02
AUB80125.1	cell division protein FtsZ	D	2.67	2.93E-02
AUB79575.1	extracellular solute-binding protein, family 3	E	2.62	4.44E-02
AUB81750.1	decarboxylase	E	2.63	2.93E-02
AUB83785.1	4-hydroxy-tetrahydrodipicolinate synthase	E	2.94	4.18E-03
AUB84954.1	acetolactate synthase	E	2.76	1.95E-02
AUB84325.1	proline iminopeptidase	E	2.91	4.18E-03
AUB82337.1	adenylosuccinate synthase	F	2.54	4.44E-02
AUB79762.1	ubiquinone biosynthesis regulatory protein kinase UbiB	H	2.86	1.23E-02
AUB80927.1	uBA THIF-type NAD FAD binding	H	2.64	2.93E-02
AUB83525.1	synthase	I	5.36	6.66E-10
AUB81024.1	lysyl-tRNA synthetase	J	3.31	1.29E-03
AUB79657.1	OmpA MotB	M	5.26	9.24E-09
AUB80121.1	cell wall formation (By similarity)	M	3.04	3.81E-03
AUB83127.1	choloylglycine hydrolase	M	2.98	3.81E-03
AUB83783.1	conserved repeat domain protein	M	2.58	4.44E-02
AUB83066.1	twitching motility protein	N, U	3.14	3.81E-03
AUB79946.1	heat-shock protein	O	2.65	2.93E-02
AUB82608.1	endopeptidase La	O	5.02	1.01E-07
AUB85620.1	DnaK-related protein	O	2.78	1.23E-02
AUB81090.1	protein of unknown function (DUF971)	S	3.55	2.26E-04
AUB82842.1	dinitrogenase iron-molybdenum cofactor biosynthesis protein	S	3.30	3.81E-03
AUB83253.1	nitrogen fixation protein	S	2.96	3.81E-03
AUB83860.1	tellurite resistance protein TehB	S	2.76	1.23E-02
AUB83943.1	short-chain dehydrogenase reductase SDR	S	2.91	4.18E-03
AUB84318.1	transposase	S	2.99	3.81E-03
AUB84331.1	dienelactone hydrolase	S	2.91	4.18E-03
AUB85354.1	protein of unknown function (DUF2868)	S	3.78	2.26E-04
AUB82296.1	Ppx GppA phosphatase	T	2.79	1.23E-02
AUB82910.1	YciI-like protein	T	2.63	2.93E-02
AUB79943.1	general secretion pathway protein G	U	2.96	3.81E-03
AUB80110.1	hypothetical protein	-	3.21	3.81E-03
AUB81753.1	ATPase	-	4.76	1.20E-06
AUB82624.1	hypothetical protein	-	2.81	1.23E-02
AUB82926.1	hypothetical protein	-	2.99	3.81E-03

1001

1002

-33-

1003　# 10.2. Figures
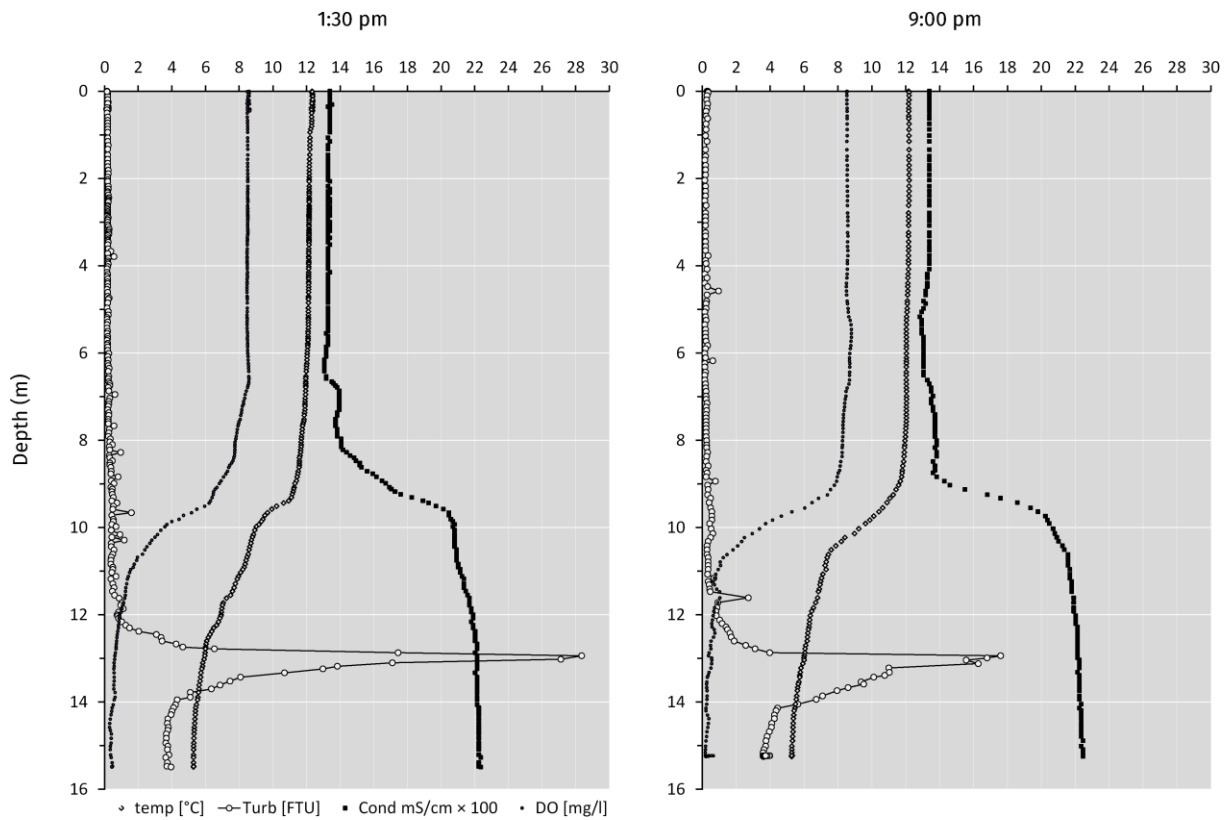
1004

1005 **Figure 1 | Conductivity, temperature, depth (CTD) profiles from Lake Cadagno on September 12 (1:30 pm) and (9:00 pm) 2017.**
1006 Measurements were taken from the platform. Probe was equilibrated for 5 min at 0.5 m depth before measuring.
1007 Temperature (◊), FTU: Formazin Turbidity Unit (○), Cond: Conductivity (■), DO: Dissolved Oxygen (●).
1008
1009
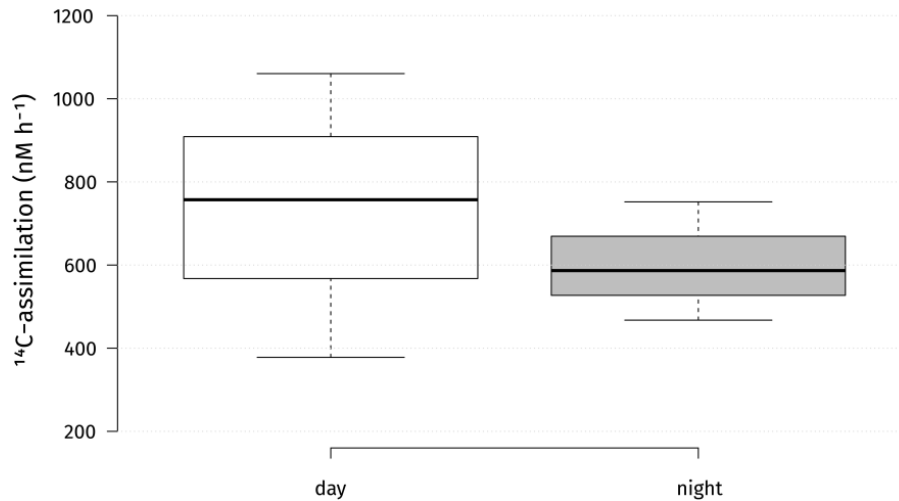
1010
1011
1012 **Figure 2| Absolute microbial ^{14}C-uptake rates in the chemocline of Lake Cadagno during day and night.** Center lines show the
1013 medians; box limits indicate the 25th and 75th percentiles as determined by *R* software; whiskers extend 1.5 times the
1014 interquartile range from the 25th and 75th percentiles, outliers are represented by dots. *n* = 3 sample points.
1015
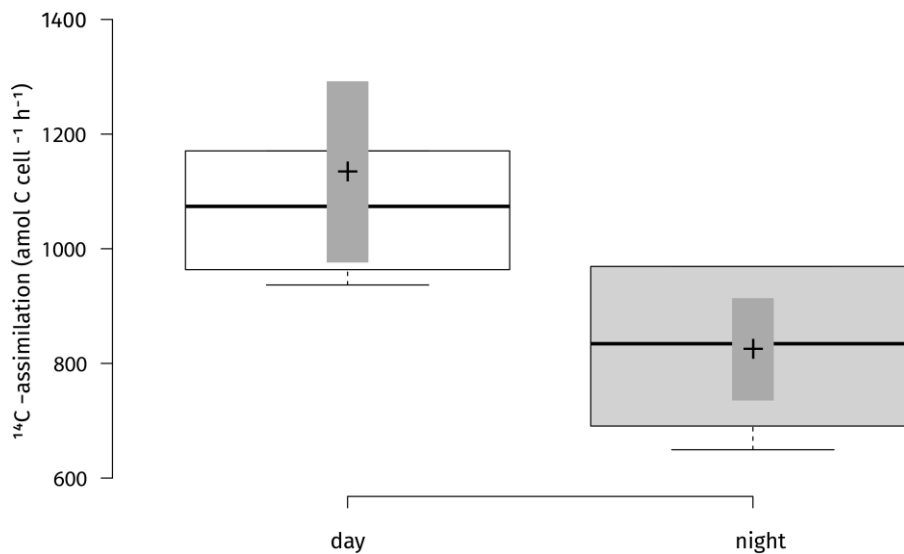
1016
1017
1018
1019
1020 **Figure 3 | Carbon uptake rates per cell for strain Cad16^T cultures for two conditions (day /night) during 4 h incubation *in*
1021 *situ*.** ^{14}C-scintillation experiments were performed on six biological replicates. Two side *t*-test statistics was applied. The
1022 difference in uptake rates between the two conditions was statistically significant at *p* <0.05 (*p* = 0.02). Center lines show the
1023 medians; box limits indicate the 25th and 75th percentiles as determined by *R* software; whiskers extend 1.5 times the
1024 interquartile range from the 25th and 75th percentiles, outliers are represented by dots; crosses represent sample means;
1025 bars indicate 83% confidence intervals of the means; data points are plotted as open circles. *n* = 6 sample points.
1026

-35-

1027 **11. APPENDIX**

1028 ## 11.1. Supplementary Tables

1029 **Table S 1| Absolute carbon uptake rates of the microbial community in the Lake Cadagno chemocline.**

	Conditions				
	light		dark		
Photosynthesis	**oxygenic**	**anoxygenic**		**depth [m]**	**Reference**
	3'825	4'175	7'608	11.5	Camacho *et al.* 2001 [30]
Carbon Uptake Rates [nM h⁻¹]	1'200		-	11.5	Musat *et al.* 2008 [33]
	85		25	12.5	Halm *et al.* 2009 [61]
	6'187		4'812	12.0	Storelli *et al.* 2013 [31]
	987		-	11.4	Berg *et al.* 2016 [38]
	757		587	14.5	This study

1030
1031
1032
1033
1034 |
1035

-36-

1036

11.2. Supplementary Figures

1037
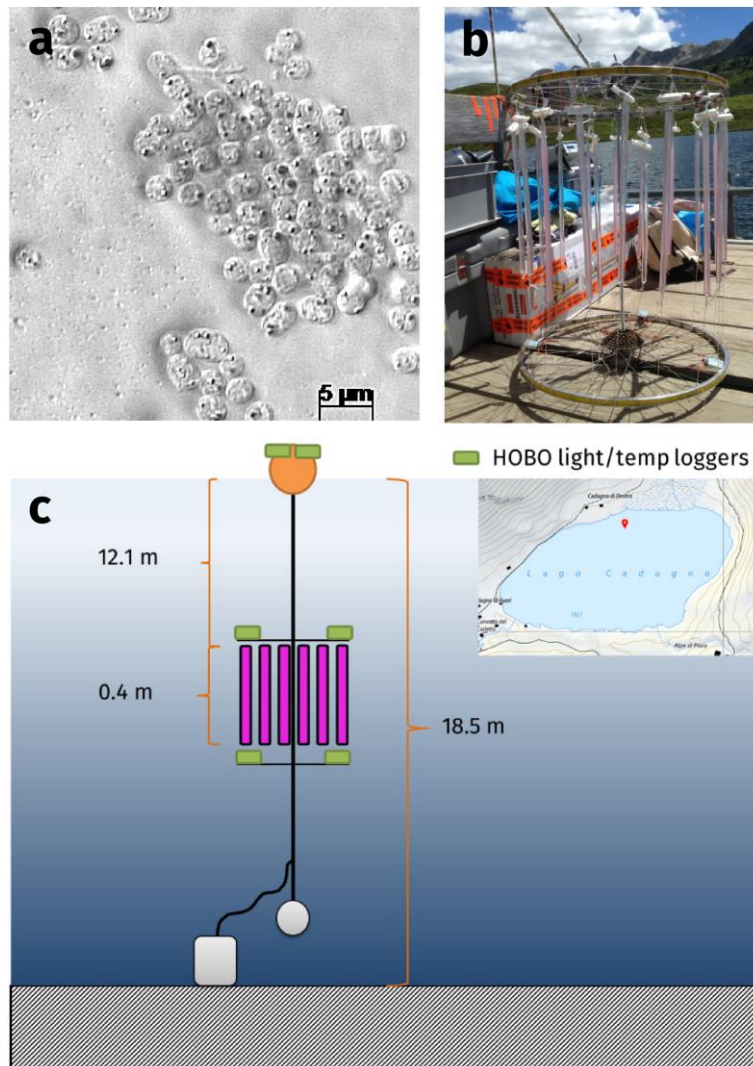
1038

1039 **Figure S 1 | Depiction of strain "*Thiodictyon syntrophicum*" sp. nov. strain Cad16^T cells, sampling site and the experimental**
1040 **setup. a)** Phase-contrast microscopic image of pure cultures of str. Cad16^T with sulfur inclusions visible as highly refractive
1041 particles. **b)** Set-up of the strain Cad16^T cultures in dialysis tubes attached to a support grid. **c)** Mooring scheme and location
1042 of the incubation experiment (initial depth, July to August) on Lake Cadagno. In pink indicated the dialysis tubes, in green
1043 the HOBO temperature and light sensors.
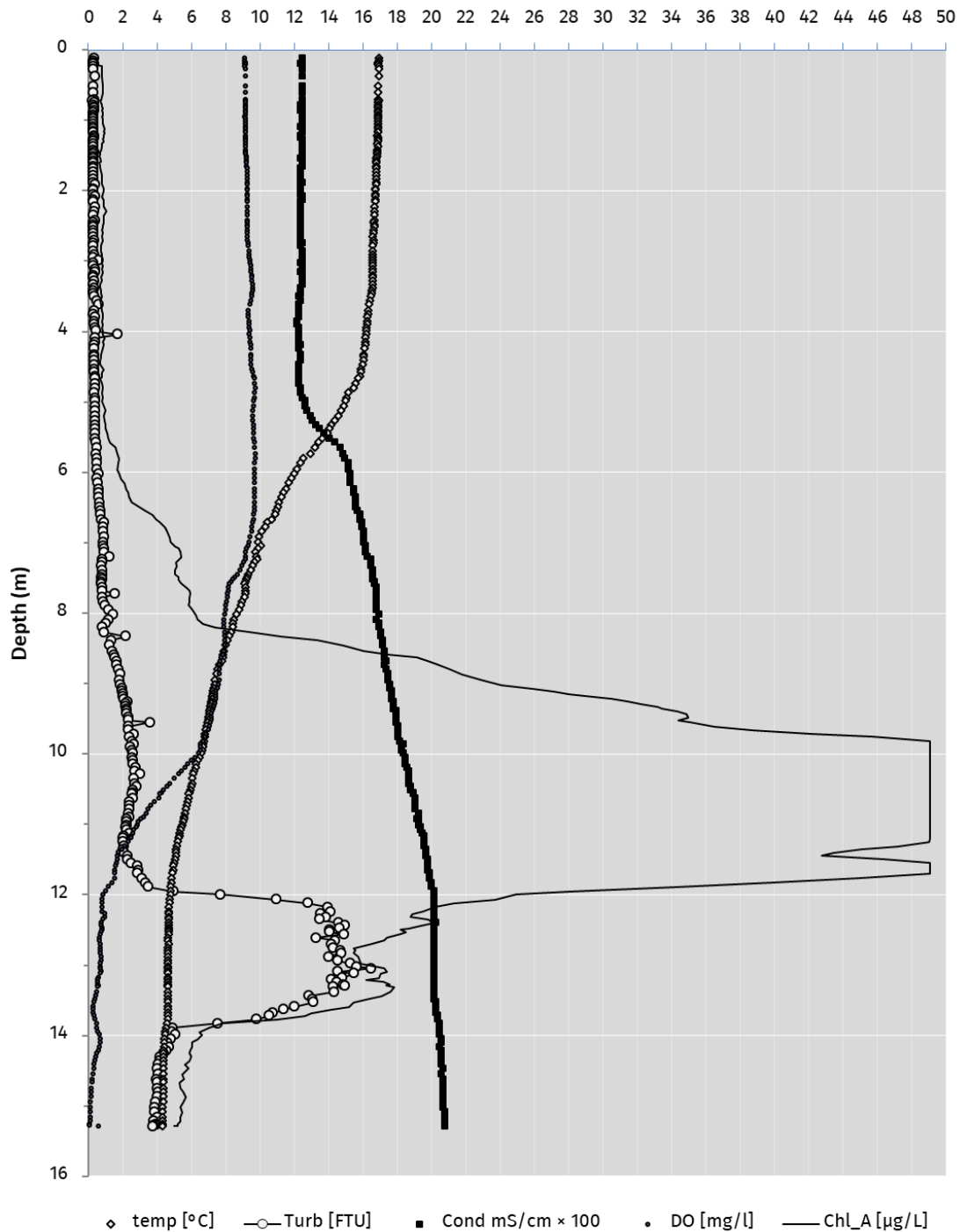
Figure S2 | Conductivity, temperature, depth (CTD) profile on July 13 2017 at 2:44 pm above the deepest point of Lake Cadagno. Chlorophyll a (——), Temperature (◊), FTU: Formazin Turbidity Unit (○), Cond: Conductivity (■), DO: Dissolved Oxygen (•),

a

b

c

1050

1051

d

-39-
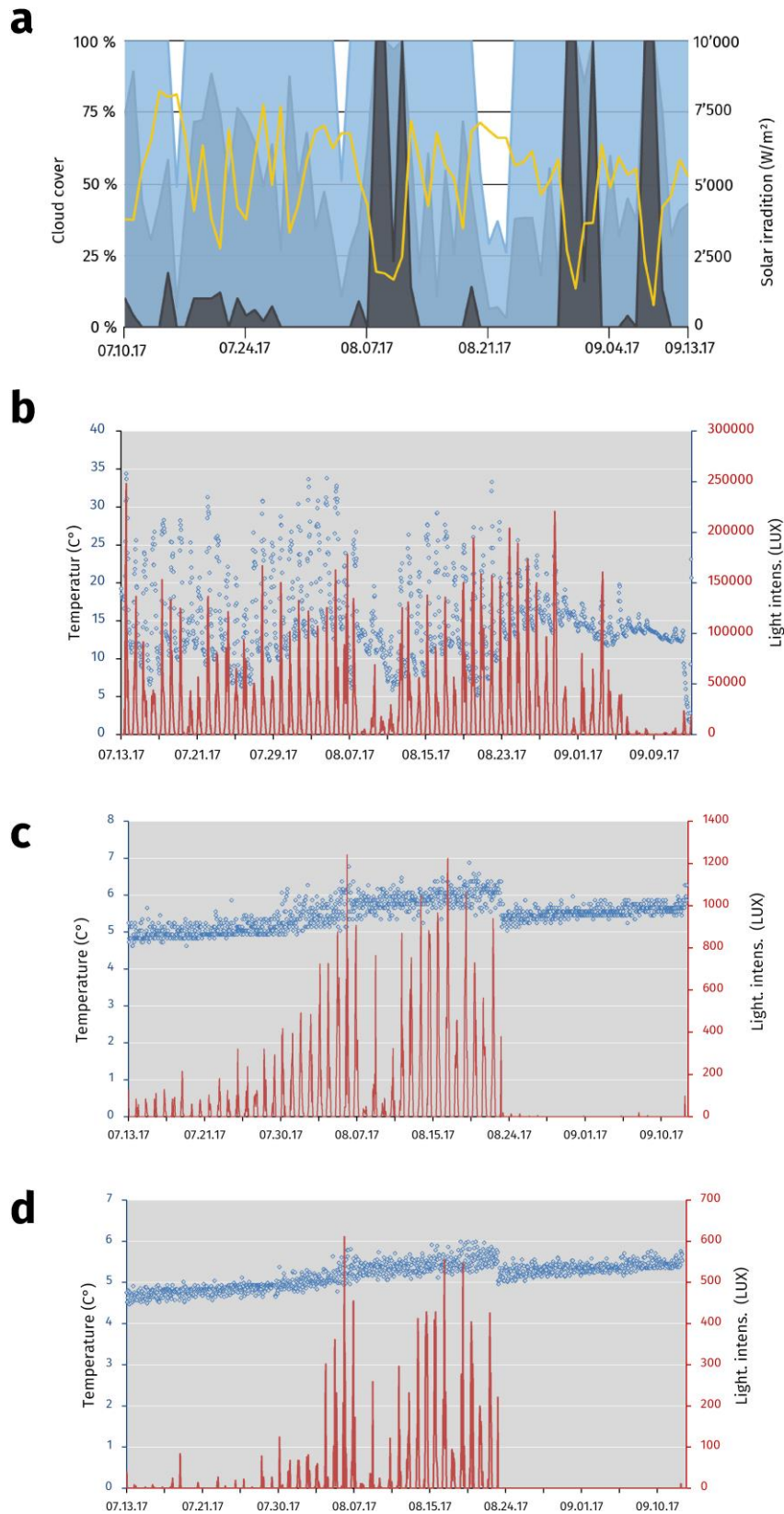
1052 **Figure S3 | Meteorological data for the Piora valley and temperature and relative light availability at different depths of the**

1053 **mooring in Lake Cadagno from July 13 to September 13 2017. a)** Sun light and cloud cover graph for the Piora valley from July

1054 13 to September 13 2017. Data from meteoblue.com (yellow; sum of the daily shortwave radiation in W m^{-2}, blue; maximal

1055 daily cloud cover in%, light blue; mean daily cloud cover in%, grey; minimal daily cloud cover in%) **b)** Temperature (black

1056 ovals) and average light available (red line) at the surface buoy of Lake Cadagno. The data logger was partly immersed in

1057 water, dampening the light and temperature readings (see values in August) **c)** A steady increase in average temperature

1058 and light availability from July to August is visible. The increase in the available light can be explained through the

1059 downward movement of photosynthetic bacteria over the season (see suppl. Fig. S5) Re-positioning of the rig on the August

1060 23 2017 results in both, a drop in temperature, and light availability. Available light was reduced to an average of 0.4 µmol m^{-}

1061 ^{2} s^{-1}. **d)** Low light availability and temperature are characteristic for the depth of around 12.4 m. As in c), temperature and

1062 available light values are steadily rising from July to August. No light was detected during daytime at 14.4 m depth after

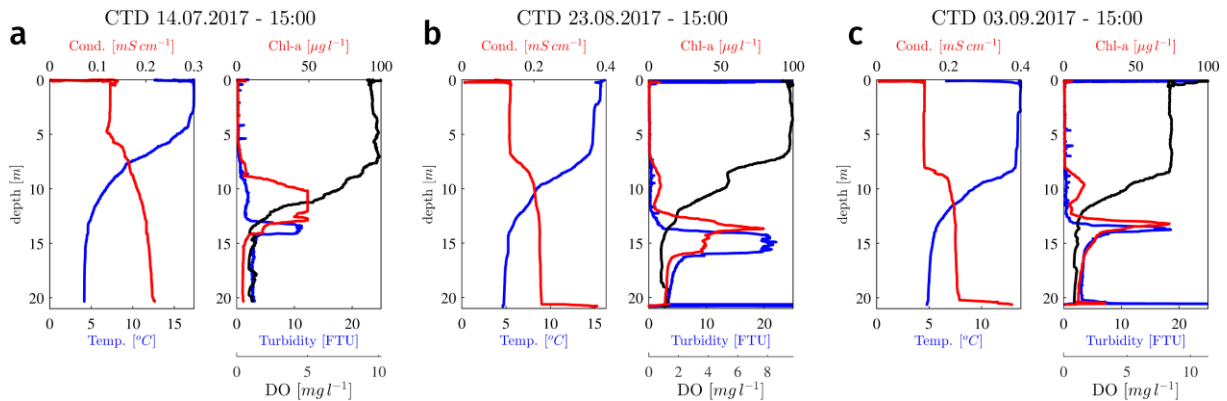1063 repositioning in August. Data was logged in hourly intervals for b)-d).

1064
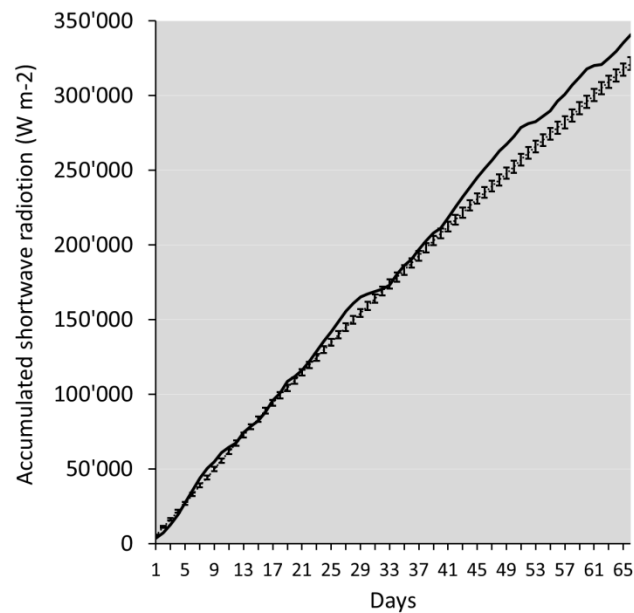
1065

1066

1067 **Figure S4 | Accumulated surface shortwave radiation for 66 days from July 10 to September 12 2017 at Piora valley**. The
1068 values for 2017 show above-average values (solid line). The mean values from 1985 to 2017 for the same time period are
1069 represented by the dotted line. Error bars indicate standard-error. Global radiation (diffuse and direct) on a horizontal
1070 plane given in Watt per square meter. Values derived from simulation data from meteoblue.com.
1071
1072

1073
1074 **Figure S5 | Vertical conductivity, temperature, depth (CTD) profiles from Lake Cadagno from July to September 2017 at the**
1075 **deepest point of the lake.** Temperature , conductivity, dissolved oxygen , chlorophyll a and turbidity are displayed for: **a)**
1076 July 14 2017 **b)** August 23 2017 **c)** September 03 2017. Formazin Turbidity Unit (FTU). The data is courtesy of Dr. Oscar
1077 Sepúlveda Steiner, Dr. Damien Bouffard and Prof. Johny Wüest. Plots courtesy of Dr. O. Sepúlveda Steiner, APHYS Laboratory,
1078 EPFL, Switzerland.
1079
1080
1081
1082
1083
1084
1085
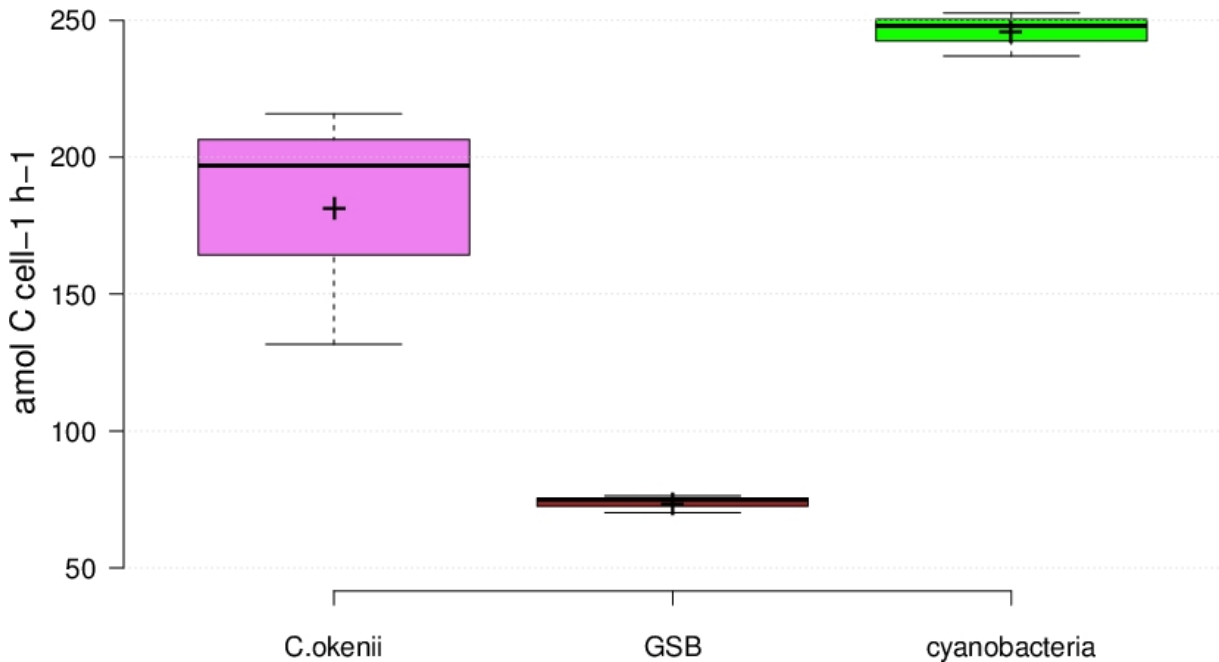
1086
1087
1088 **Figure S6 | Average inorganic uptake rates at the chemocline of the three populations counted with FCM at 1:30 pm.**
1089 *Chromatium okenii* (pink), green sulfur bacteria (GSB; brown) and cyanobacteria (green). Center lines show the medians; box
1090 limits indicate the 25th and 75th percentiles as determined by *R* software; whiskers extend 1.5 times the interquartile range
1091 from the 25th and 75th percentiles, outliers are represented by dots; crosses represent sample means. *n* = 3 sample points.
1092